Published in final edited form as:

Nature. 2019 April ; 568(7752): 405–409. doi:10.1038/s41586-019-1082-x.

Innate lymphoid cells support regulatory T cells in the intestine through interleukin-2

Lei Zhou[1,2,3], **Coco Chu**[1,2,3], **Fei Teng**[1,2,3], **Nicholas J. Bessman**[1,2,3], **Jeremy Goc**[1,2,3], **Endi K. Santosa**[3], **Gregory G. Putzel**[3], **Hiroki Kabata**[1,2,3], **Judith R. Kelsen**[4], **Robert N. Baldassano**[4], **Manish A. Shah**[5], **Robbyn E. Sockolow**[6], **Eric Vivier**[7,8], **Gérard Eberl**[9], **Kendall A. Smith**[10], **Gregory F. Sonnenberg**[1,2,3]

[1]Joan and Sanford I. Weill Department of Medicine, Division of Gastroenterology, Weill Cornell Medicine, Cornell University, New York, NY, USA

[2]Department of Microbiology and Immunology, Weill Cornell Medicine, Cornell University, New York, NY, USA

[3]Jill Roberts Institute for Research in Inflammatory Bowel Disease, Weill Cornell Medicine, Cornell University, New York, NY, USA

[4]Division of Gastroenterology, Hepatology and Nutrition, Children's Hospital of Philadelphia, and the Perelman School of Medicine, University of Pennsylvania, Philadelphia, PA, USA

[5]Weill Cornell Medicine, New York-Presbyterian Hospital, New York, NY, USA

[6]Department of Pediatrics, Division of Gastroenterology and Nutrition, Weill Cornell Medicine, Cornell University, New York, NY, USA

[7]Aix Marseille Univ, APHM, CIML, Hôpital de la Timone, Immunologie, Marseille-Immunopole, Marseille, France

[8]Innate Pharma Research Laboratories, Innate Pharma, Marseille, France

[9]Institut Pasteur, Microenvironment and Immunity Unit, Paris, France

[10]Joan and Sanford I. Weill Department of Medicine, Division of Immunology, Weill Cornell Medicine, Cornell University, New York, NY, USA

Abstract

Correspondence and requests for materials should be addressed to gfsonnenberg@med.cornell.edu.

Author contributions

L.Z. and G.F.S. conceived the project. L.Z. performed most experiments and analyzed the data. F.T., C.C., N.J.B., J.G., H.K. and E.S. helped with experiments. G.G.P. performed bioinformatics analyses. J.R.K., R.N.B., M.A.S. and R.E.S. provided human samples, scientific advice, and valuable expertise. E.V., G.E. and K.A.S. provided essential mouse models, scientific advice, and expertise. L.Z. and G.F.S. wrote the manuscript, with input from all the authors.

Data availability

RNA-seq data are available at Gene Expression Omnibus (https://www.ncbi.nlm.nih.gov/geo/) under accession number GSE126580. All data sets generated and/or analyzed during the current study are presented in this published article, the accompanying Source Data or Supplementary Information files, or are available from the corresponding author upon reasonable request.

The authors declare no competing interests.

Interleukin (IL)-2 is a pleiotropic cytokine that is necessary to prevent chronic inflammation in the gastrointestinal tract[1–4]. The protective effects of IL-2 involve the generation, maintenance and function of regulatory T cells (Tregs)[4–8], and low-dose IL-2 has emerged as a potential therapeutic strategy in inflammatory bowel disease (IBD) patients[9]. However, the cellular and molecular pathways that control the production of IL-2 in the context of intestinal health are undefined. Here we identify that IL-2 is acutely required to maintain Tregs and immunologic homeostasis throughout the gastrointestinal tract. Strikingly, lineage-specific deletion of IL-2 in T cells did not recapitulate these phenotypes in the small intestine. Unbiased analyses revealed that group 3 innate lymphoid cells (ILC3) are the dominant cellular source of IL-2 in the small intestine, which is selectively induced by IL-1β. Macrophages produce IL-1β in the small intestine and activation of this pathway involves MyD88- and Nod2-dependent sensing of the microbiota. Loss-of-function studies defined that ILC3-derived IL-2 is essential to maintain Tregs, immunologic homeostasis and oral tolerance to dietary antigens uniquely in the small intestine. Furthermore, ILC3 production of IL-2 was significantly reduced in the small intestine of Crohn's disease patients, and this correlated with diminished Tregs. Collectively, these results reveal a previously unappreciated pathway whereby a microbiota- and IL-1β-dependent axis promotes ILC3 production of IL-2 to orchestrate immune regulation in the intestine.

To determine whether IL-2 is constitutively required for the maintenance of Tregs and immunologic homeostasis in the intestine, we administered isotype control or anti-IL-2 neutralizing antibodies every other day to adult mice for two weeks. Within this short time period, neutralization of IL-2 promoted an enlargement of the spleen and mesenteric lymph nodes (mLN), and caused significant reductions of Tregs and increases in the proliferation of $CD4^+$ T cells throughout the gastrointestinal tract and associated lymphoid tissues, including the mLN, large intestine and small intestine (Extended Data Fig. 1a–g). Further, blockade of IL-2 resulted in significantly enhanced IFNγ production by $CD4^+$ T cells in both the small and large intestine, as well as more IL-17A production in the large intestine (Extended Data Fig. 1h–k). Previous studies have suggested that $CD4^+$ T cells are the dominant cellular source of IL-2[1,2]. Therefore, we generated mice with a lineage-specific deletion of IL-2 in T cells by crossing IL-2-floxed mice[10] with Lck^{cre} mice. Lck^{cre}-$Il2^{f/f}$ mice exhibited a complete loss of IL-2 protein staining in T cells, and we observed a significant reduction of Tregs, an increase in $CD4^+$ T cell proliferation and effector function in the mLN and large intestine (Extended Data Fig. 2a–g). In contrast, deletion of T cell-derived IL-2 did not alter Tregs, $CD4^+$ T cell proliferation, or effector cytokine production within the small intestine (Extended Data Fig. 2h–k). Collectively, these data demonstrate that T cell-derived IL-2 is required for maintaining immunologic homeostasis in lymphoid tissues and the large intestine, but is dispensable in the small intestine, indicating the existence of other critical cellular sources of IL-2.

We next sought to examine the relevant cellular sources of IL-2 in the healthy mammalian small intestine by unbiased flow cytometry analyses. Notably, we observed that the major population of $IL\text{-}2^+$ cells lack lineage markers for T cells, B cells, macrophages and dendritic cells (DCs), but are $CD127^+$, $CD90.2^+$ and express retinoic acid–related orphan receptor γ t (RORγt) (Fig. 1a), a phenotype consistent with group 3 innate lymphoid cells (ILC3)[11–13]. To directly compare *Il2* transcript levels between $CD4^+$ T cells and ILC3 in the

healthy small intestine, we performed RNA sequencing on sorted cell populations. In comparison to differentially expressed genes found in ILC3 (*Rorc*, *Il22*, *Il1r* and *Il23r*) or CD4$^+$ T cells (*Cd3d*), *Il2* expression was more highly enriched in ILC3 (Fig. 1b). Significantly higher expression of *Il2* was confirmed in ILC3 relative to CD4$^+$ T cells, DCs or B cells following quantitative PCR analysis of populations purified from the healthy mouse small intestine (Fig. 1c). Furthermore, ILC3 were the most abundant IL-2$^+$ cell type in terms of frequency and total cell number among other innate lymphoid cell (ILC) subsets and total CD4$^+$ T cells from the small intestine (Fig. 1d–f, Extended Data Fig. 3), as well as higher cell numbers than effector/memory CD4$^+$ T cells (Extended Data Fig. 4a). This is in contrast to the large intestine, where the majority of IL-2 was produced by CD4$^+$ T cells and there was a limited presence of IL-2-producing ILCs (Extended Data Fig. 4b–d). ILC3 are a heterogeneous population, including both CCR6$^+$ lymphoid tissue inducer (LTi)-like ILC3s and T-bet$^+$ ILC3s[11–13]. IL-2 in the small intestine was produced by both ILC3 subsets, with a significantly higher frequency of IL-2-producing ILC3 that co-express T-bet (Extended Data Fig. 4e). Production of IL-2 by ILC3 was confirmed by flow cytometry analyses of the small intestine of *Rag1*$^{-/-}$ mice, revealing that the major population of IL-2$^+$ cells is CD127$^+$ CD90.2$^+$ RORγt$^+$ ILC3 (Extended Data Fig. 4f–h), consisting of both T-bet$^+$ ILC3 and CCR6$^+$ ILC3 (Extended Data Fig. 4i, j). Unbiased analyses of the large intestine of *Rag1*$^{-/-}$ mice indicated that the major population of IL-2$^+$ cells are ILCs (Extended Data Fig. 4k). Further, the IL-2$^+$ cells observed in the small intestine of *Rag2*$^{-/-}$ mice were significantly reduced in ILC-deficient *Rag2*$^{-/-}$*Il2rg*$^{-/-}$ mice or *Rag2*$^{-/-}$ mice depleted of ILCs with anti-CD90.2 antibody (Fig. 1g). Collectively, these findings define that IL-2 is dominantly produced by ILC3 in the healthy small intestine.

ILC3 development and function can be dramatically influenced by the intestinal microbiota[11–13]. To interrogate whether this also regulates ILC3-intrinsic IL-2 production, we examined the small intestine of conventionally housed specific pathogen free (SPF) mice, SPF mice exposed to broad-spectrum antibiotics (ABX), and germ free (GF) mice. Strikingly, GF mice or ABX mice displayed significantly decreased IL-2 production by ILC3 relative to SPF mice (Fig. 2a). To determine what signals directly induce ILC3-intrinsic IL-2 production, we stimulated sort-purified ILC3 from the small intestine with IL-1β, IL-6, IL-23, or the aryl hydrocarbon receptor agonist FICZ, which are all known to directly stimulate ILC3[11–13]. Among these, we found that IL-1β selectively induced *Il2* transcription and protein production in ILC3 (Fig. 2b, c). We observed comparable results with IL-1α stimulation (Fig. 2d). Furthermore, IL-1β was sufficient to significantly boost IL-2 production in ILC3 from ABX mice and GF mice (Fig. 2e, f).

Gene expression analyses of intestinal phagocytes revealed that the majority of IL-1β in the small intestine is produced by macrophages (Fig. 2g). Consistent with this, macrophages isolated from the small intestine of germ free mice exhibited significantly reduced IL-1β expression, and could be partially restored by mono-colonization with segmented filamentous bacteria (SFB; Fig. 2h), a component of the mouse microbiota known to colonize the distal small intestine, induce IL-1β, activate ILC3, and promote Treg expansion[14–16]. Further, mono-colonization with SFB was sufficient to significantly induce ILC3-derived IL-2 production (Fig. 2i). To explore the sensing modules that are required to promote the IL-1β-ILC3-IL-2 axis, we examined *Myd88*$^{-/-}$ mice and observed a significant

reduction in macrophage expression of IL-1β (Fig. 2j). The intracellular pattern recognition receptor Nod2 has also been linked to the processing and secretion of IL-1β[17]. Consistent with this, we observed comparable transcript levels of IL-1β in macrophages sorted from the small intestine of *Nod2*$^{-/-}$ mice, but ILC3-derived IL-2 was significantly reduced and could be completely restored by stimulation with recombinant IL-1β (Fig. 2j, k). These data reveal that MyD88- and Nod2-dependent sensing of the intestinal microbiota is essential to promote macrophage production of IL-1β and activate ILC3 to produce IL-2.

To directly investigate whether IL-1R signaling is essential for IL-2 production by ILC3 *in vivo*, we crossed *Ncr1*^{cre} and IL-1R-floxed mice, to selectively delete IL-1R on the NKp46^{+} ILC3 subset[18,19]. In comparison to littermate control mice, *Ncr1*^{cre}-*Il1r*$^{f/f}$ mice exhibit reduced IL-2 production by ILC3 and display a significant decrease of Tregs in the small intestine (Fig. 3a, b). To directly interrogate the role of ILC3-derived IL-2, we generated mice with a deletion of IL-2 in ILC3 by employing *Ncr1*^{cre}-*Il2*$^{f/f}$ mice. This approach resulted in an efficient loss of IL-2 in T-bet^{+} ILC3 in the small intestine, but did not alter the frequency of IL-2 production in CD4^{+} T cells or DCs (Extended Data Fig. 5a). Further, we observed minimal production of IL-2 in NK cells and ILC1 in the small intestine, and these populations do not contribute to Treg homeostasis as no changes were observed following depletion with anti-NK1.1 antibody (Extended Data Fig. 5b–d). In contrast, we observed a significant reduction in the frequency and number of Tregs in the small intestine of *Ncr1*^{cre}-*Il2*$^{f/f}$ mice as compared to littermate controls (Fig. 3c, Extended Data Fig. 6a). The reduction of Treg cells was associated with a significant increase of Th1 cells, whereas Th17 cells and the proliferation of CD4^{+} T cells were unchanged (Fig. 3d, Extended Data Fig. 6b–d). These results were tissue-specific, as no changes in Tregs were observed in the large intestine of *Ncr1*^{cre}-*Il2*$^{f/f}$ mice, and further no changes were observed in ILC3 homeostasis or cytokine production in the small intestine of *Ncr1*^{cre}-*Il2*$^{f/f}$ mice (Extended Data Fig. 6e–g). This was surprising given that ILC3 can respond to IL-2, however, we observed that Tregs exhibit higher levels of the high affinity IL-2R (CD25) and more efficiently bind IL-2 relative to ILC3 from the small intestine (Extended Data Fig. 6h, i).

Loss of ILC3-specific IL-1R or IL-2 significantly reduced the frequencies of peripherally-induced Tregs in the small intestine, marked by low staining of neuropilin-1, in addition to significant reductions of both RORγt^{+} and GATA3^{+} Treg subsets (Extended Data Fig. 7a–d). ILC3-derived IL-2 did not impact Treg expression of *Lag3, Tgfb1, Ctla4*, and *Ebi3*, but did result in a modest decrease in *Il10* (Extended Data Fig. 7e). Consistent with this, Tregs from the small intestine of control and *Ncr1*^{cre}-*Il2*$^{f/f}$ mice exhibited comparable potential to suppress effector T cell proliferation when ratios were normalized (Extended Data Fig. 7f, g). Furthermore, prior studies identified a role for ILC3 in regulating adaptive immunity in the large intestine through GM-CSF and MHCII[20–22]. However, loss of GM-CSF or ILC3-specific MHCII did not impact Tregs in the small intestine or IL-2 production by ILC3, and similarly ILC3-derived IL-2 did not impact ILC3 expression of GM-CSF or MHCII (Extended Data Fig. 8)[34]. These data collectively demonstrate that ILC3-derived IL-2 is a novel and non-redundant pathway that supports the population size and homeostasis of peripherally-induced Tregs in the small intestine.

Peripheral Tregs in the small intestine are induced by dietary antigens and maintain oral tolerance[23]. Therefore, we next asked whether deficiency of ILC3-intrinsic IL-2 affects the *de novo* maintenance of small intestinal Tregs upon oral administration of ovalbumin (OVA). Notably, the induction of OVA-specific inducible Tregs (Nrp-1^{lo}) in the small intestine was significantly impaired in *Ncr1*^{cre}-*Il2*$^{f/f}$ mice as compared to littermate controls (Fig. 3e). Further, we assessed whether oral tolerance was intact in these mice with a delayed-type hypersensitivity (DTH) model[24]. In contrast to littermate controls, OVA feeding to *Ncr1*^{cre}-*Il2*$^{f/f}$ mice failed to induce oral tolerance and did not protect mice from a DTH reaction characterized by ear swelling and higher titers of anti-OVA immunoglobulin G1 (IgG1) in the serum upon OVA challenge in the periphery (Fig. 3f, g, Extended Data Fig. 6j). These data are consistent with prior literature describing that a critical step in oral tolerance is maintenance and expansion of antigen-specific Tregs in the lamina propria of the intestine[25]. Further these data critically demonstrate that NKp46^{+} ILC3 are an essential and non-redundant source of IL-2 for maintaining Treg homeostasis and promoting oral tolerance uniquely in the small intestine.

We next targeted IL-2 in all ILC3 subsets by generating *Rorc*^{cre}-*Il2*$^{f/f}$-*Rag1*$^{-/-}$ mice and associated controls, and reconstituted these mice with an adoptive transfer of unfractionated wild-type CD4^{+} T cells. Surprisingly, in comparison to *Il2*$^{f/f}$-*Rag1*$^{-/-}$ recipients, *Rorc*^{cre}-*Il2*$^{f/f}$-*Rag1*$^{-/-}$ recipients exhibited rapid and substantial weight loss, shorter colon length, spontaneous colonic inflammation characterized by elevated inflammatory cell infiltration, and significantly elevated levels of fecal Lipocalin-2 (Extended Data Fig. 9a–d). Notably, we observed significantly decreased colonic Tregs, associated with significantly increased IL-17A^{+}IFNγ^{-} and IL-17A^{+}IFNγ^{+} T cells in the large intestine, as well as increased Th1 cells in the small intestine of *Rorc*^{cre}-*Il2*$^{f/f}$-*Rag1*$^{-/-}$ recipients relative to controls, even though both groups exhibited comparable small intestinal Tregs (Extended Data Fig. 9e–h). These findings provoke a model whereby ILC3-derived IL-2 can also modulate immunologic homeostasis and prevent inflammation throughout the entire gastrointestinal tract in the context of lymphopenia.

Finally, to interrogate whether ILC3s support Tregs in the human intestine, we examined the frequency of these populations in intestinal biopsies from healthy controls and Crohn's disease patients. As previously reported[26,27], we observed significantly reduced frequencies of Tregs and ILC3 in the small intestine of Crohn's disease patients relative to healthy controls, and strikingly, we also identified a significant positive correlation between the frequencies of these two cell types within the same biopsy (Fig. 4a–c). To determine whether the impaired Treg responses are associated with reduced ILC3-derived IL-2, we sort purified ILC3 from resected small intestinal tissues of Crohn's disease patients and identified significantly reduced *IL2* transcript when isolated from inflamed versus non-inflamed regions (Fig. 4d). In addition, IL-2^{+} ILC3s were significantly reduced in terminal ileum biopsies from Crohn's disease patients relative to healthy controls, and no significant change was observed in IL-2^{+} CD4^{+} T cells (Fig. 4e, f). These data indicate that similar to mice, ILC3 support Tregs within the human small intestine, and further that this pathway becomes dysregulated in the context of Crohn's disease.

Collectively, results from these studies identify a novel pathway of immune regulation that uniquely occurs in the healthy small intestine (Extended data Fig. 10). This pathway is continuously required, involves MyD88- and Nod2-dependent microbial sensing by macrophages, production of IL-1β, and induction of ILC3-derived IL-2. Subsequently, this pathway supports intestinal Tregs, immunologic homeostasis and oral tolerance. These findings translated into human samples and indicate that impaired ILC3-derived IL-2 is linked to a reduction of Tregs and impaired immune regulation within the small intestine of Crohn's disease patients. Our results will inform ongoing strategies of therapeutically administering low-dose IL-2 to IBD patients, or in the context of individuals with lymphopenia, immune-deficiencies or following treatment with chemo-toxic agents. ILC3-derived IL-2 does not exhibit functional redundancy or hierarchies with previously known pathways by which ILC3 regulate adaptive immunity in the large intestine. Rather these data define anatomical differences in the mechanisms by which ILC3 orchestrate immune tolerance in the small versus large intestine. This likely is driven by substantial differences in microbial burdens, mucus layers, tissue permeability and metabolite access between these two organs[28–30]. These new data are critically important as a great deal is known on the mechanisms that support Tregs in the large intestine[4–8,30], while less is known about the pathways supporting Tregs in the small intestine. Finally, our results substantially advance our understanding of the role and regulation of IL-2 throughout the gastrointestinal tract, and critically identify a previously unappreciated direct communication between ILC3 and Tregs.

Methods

Mice

Wild-type, *Rag1*$^{-/-}$, Thy1.1, OT-II, *Lck*^{cre}, *Il1r*$^{f/f}$, *H2-Ab1*$^{f/f}$, *Csf2*$^{-/-}$, *Myd88*$^{-/-}$ and *Nod2*$^{-/-}$ mice on a C57BL/6 background were purchased from the Jackson Laboratory. *Rag2*$^{-/-}$ and *Rag2*$^{-/-}$*Il2rg*$^{-/-}$ on a C57BL/6 background were purchased from Taconic Farms. C57BL/6 *Rorc*^{cre} mice and *Rorc(γt)-Gfp*^{TG} mice were provided by G. Eberl. C57BL/6 *Il2*$^{f/f}$ mice were provided by K. A. Smith. C57BL/6 *Ncr1*^{cre} were provided by E. Vivier and only heterozygous *Ncr1*^{cre} mice were utilized in this study. All mice were bred and maintained in specific pathogen-free facilities at Weill Cornell Medicine and littermates were used as controls in all experiments. C57BL/6 germ free mice were maintained at the gnotobiotic facility at Weill Cornell Medicine. Sex- and age-matched animals between 8 and 14 weeks of age were used for experiments if not otherwise indicated. Gender was not found to influence results of any experiments. No animals were excluded from the analysis unless clearly indicated. All animal experiments were approved and are in accordance with the Institutional Animal Care and Use Committee guidelines at Weill Cornell Medicine.

In vivo administration of antibodies and antibiotics

Anti-IL-2 monoclonal antibodies (JES6–1A12 and S4B6–1, BioXCell) were administered intraperitoneally every other day at a dose of 300 μg (150 μg JES6–1A12 plus 150 μg S4B6–1) per mouse starting on day 0 and ending on day 14. Anti-CD90.2 monoclonal antibody (30H12, BioXCell) was administered intraperitoneally every 3 days at a dose of 250 μg per mouse starting on day 0 and ending on day 14, as previously described[21]. Anti-NK1.1

monoclonal antibody (PK136, BioXCell) was administered intraperitoneally every 3 days at a dose of 250 μg per mouse starting on day 0 and ending on day 14. A cocktail of antibiotics (0.25 mg/mL of vancomycin, 0.5 mg/mL of ampicillin, neomycin, gentamicin and metronidazole, and 4 mg/mL sucralose) was continuously administered via drinking water for 2 weeks.

Isolation of cells from the intestinal lamina propria of mice and humans

Intestines were removed, cleaned from remaining fat tissue and washed in ice-cold PBS (Corning). Peyer's patches on the small intestine were identified and removed. Intestines were opened longitudinally and washed in ice-cold PBS. Afterwards, mucus was gently removed by forceps and intestines were cut into approximately 0.5 cm sections. Dissociation of epithelial cells was performed by incubation on a shaker in HBSS (Sigma-Aldrich) containing 5 mM EDTA (Thermo Fisher Scientific), 1 mM DTT (Sigma-Aldrich) and 2% FBS two times for 20 min at 37 °C. After each step, samples were vortexed and the epithelial fraction discarded. Afterwards, samples were washed by PBS and enzymatic digestion was performed in RPMI containing 10% FBS and 0.4 U/mL dispase (Thermo Fisher Scientific), 1 mg/mL collagenase III (Worthington) and 20 μg/mL DNase I (Sigma-Aldrich) on a shaker for 45 min at 37 °C. Leukocytes were further enriched by a 40/80% Percoll gradient centrifugation (GE Healthcare).

For human samples, de-identified intestinal biopsies from the terminal ileum of pediatric individuals with Crohn's disease or age matched non-IBD controls were obtained following Institutional Review Board approved protocols from either the Children's Hospital of Philadelphia or the JRI IBD Live Cell Bank Consortium at Weill Cornell Medicine. Informed consent was obtained from all subjects. Tissues were processed by first incubating in 1 mM EDTA, 1 mM DTT and 5% FBS (all from Thermo Fisher Scientific) for 30 min at 37 °C with shaking to remove intestinal epithelial cells. Supernatants were then discarded and the remaining tissues were incubated in 0.5 mg/mL collagenase and 20 μg/mL DNase I for 30 min at 37 °C with shaking to obtain the lamina propria fraction. Any remaining tissues were also included following mechanical dissociation and filtering through a 70 μm cell strainer. All cells were then viably cryopreserved at −150 °C in 90% FBS and 10% DMSO for future side-by-side analyses.

Surgical resection samples from the small intestine of Crohn's disease patients were obtained through Institutional Review Board approved protocols from the Centers for Advanced Digestive Care at Weill Cornell Medicine. Informed consent was obtained from all subjects. Inflamed and non-inflamed regions were isolated by a trained pathologist. Single cell suspensions from intestinal tissues were obtained by incubating tissues for 30 min at 37°C with shaking in stripping buffer (1 mM EDTA, 1 mM DTT and 5% FCS) to remove the epithelial layer. Supernatants were then discarded. Tissues were then mechanically dissociated with a sterile scalpel. The lamina propria fraction was obtained by incubating the dissociated tissues for 1 hour at 37°C with shaking in 2 mg/ml collagenase D (Roche), 0.1 mg/mL DNase I (Sigma) and 1 mg/mL of Trypsin Inhibitor (Gibco) digestion solution. Remaining tissues were then filtered through a 70 μm cell strainer. All cells were then viably cryopreserved in 90% FBS and 10% DMSO for side-by-side analysis at a later

time point. Following thawing and filtering through a 70 μm cell strainer, cells were stained with antibodies for flow cytometry acquisition.

Flow cytometry and cell sorting

Single cell suspensions were incubated on ice with conjugated antibodies in PBS containing 2% FBS and 1 mM EDTA. Dead cells were excluded with Fixable Aqua Dead Cell Stain (Thermo Fisher Scientific). The staining antibodies for flow cytometry were purchased from Thermo Fisher Scientific, Biolegend or BD Biosciences. For mouse cell-surface staining: B220 (RA3–6B2), CCR6 (29–2L17), CD3ε (145–2C11), CD4 (GK1.5 or RM4–5), CD5 (53–7.3), CD8α (53–6.7), CD11b (M1/70), CD11c (N418), CD19 (eBio1D3), CD25 (PC61.5), CD44 (IM7), CD45 (30-F11), CD45RB (C363–16A), CD62L (MEL-14), CD64 (X54–5/7.1), CD90.2 (30-H12), CD127 (A7R34), CD172a (P84), F4/80 (BM8), MHC II (M5/114.15.2), NK1.1 (PK136), Nrp-1 (3E12), TCRβ (H57–597), Thy1.1 (OX-7) and XCR1 (ZET). For mouse intracellular staining: Eomes (Dan11mag), Foxp3 (FJK-16S), GATA3 (L50–823), GM-CSF (MP1–22E9), IL-2 (JES6–5H4), IL-6 (MP5–20F3), IL-17A (eBio 17B7), IL-22 (IL22JOP), IFNγ (XMG1.2), Ki-67 (SolA15), RORγt (B2D or Q31–378), T-bet (eBio4B10) and TNFα (MP6-XT22). Human samples were stained for CD3 (UCHT1), CD4 (SK3), CD5 (UCHT2), CD11b (CBRM1/5), CD11c (3.9), CD14 (TuK4), CD19 (HIB19), CD34 (581), CD45 (HI30), CD94 (DX22), CD117 (104D2), CD123 (6H6), CD127 (A019D5), FcεR1 (AER-37), Foxp3 (PCH101), IL-2 (MQ1–17H12) and NKp44 (44.189).

For intracellular transcription factor or cytokine staining, cells were stained for surface markers, followed by fixation and permeabilization according to the manufacturer's protocol (Foxp3 staining buffer set from Thermo Fisher Scientific). For intracellular cytokine staining, cells were first incubated for 4 hours in RPMI with 10% FBS, 50 ng/mL phorbol 12-myristate 13-acetate (PMA), 750 ng/mL ionomycin and 10 μg/mL brefeldin A, all obtained from Sigma-Aldrich. IL-2 binding capacity was assessed using a biotinylated IL-2 Fluorokine assay kit (R&D Systems), following manufacturer's instructions. All flow cytometry experiments were performed using a Fortessa II flow cytometer and the FACS Diva software (BD Biosciences) and analyzed with FlowJo V10 software (TreeStar) or sort-purified by using FACSAria II cell sorter (BD Biosciences).

T cell adoptive transfer

1×10^6 naïve OT-II T cells ($CD4^+CD25^-CD44^{lo}CD62L^{hi}$) were sort-purified from the spleen and lymph nodes of $Thy1.1^+$OT-II mice and adoptively transferred by retro-orbital injection into recipients (*Il2*$^{f/f}$ and *Ncr1*^{cre}-*Il2*$^{f/f}$ mice). One day later, recipient mice were gavaged with OVA (grade V, Sigma-Aldrich) 20 mg per mouse every other day and simultaneously fed *ad libitum* with OVA dissolved in drinking water (10 mg/ml) for 12 days. Treg conversion of naïve OT-II cells was analyzed in the small intestine on day 13.

$CD3^+CD4^+$ T cells were sorted from the spleen and lymph nodes of $Thy1.1^+$ mice mice and 3×10^6 cells were transferred intravenously to each recipient mouse (*Il2*$^{f/f}$-*Rag1*$^{-/-}$ and *Rorc*^{cre}-*Il2*$^{f/f}$-*Rag1*$^{-/-}$ mice). Weights of recipient mice were monitored through the progression of the experiment.

In vitro stimulation

Sort-purified ILC3 ($CD45^+CD3^-ROR\gamma t^{GFP+}CD127^+$) from small intestine of *Rorc(γt)-Gfp*^{TG} mice were plated in a 96-well plate (1×10^4 cells per well for quantitative PCR or 2×10^4 cells per well for ELISA) and incubated in DMEM with high glucose supplemented with 10% FBS, 10 mM HEPES, 1 mM sodium pyruvate, non-essential amino acids, 80 μM 2-mercaptoethanol, 2 mM glutamine, 100 U/ml penicillin and 100 μg/ml streptomycin (all from Gibco) in the presence of recombinant mouse IL-1β (20 ng/ml, Thermo Fisher Scientific), IL-6 (20 ng/ml, Thermo Fisher Scientific), IL-23 (20 ng/ml, Thermo Fisher Scientific) or FICZ (500 nM, Sigma-Aldrich) at 37 °C. For quantitative PCR, cells were treated for 4 hours, for ELISA, cells were stimulated for 24 hours in the presence of PMA (25 ng/ml) and ionomycin (375 ng/ml).

Induction and measurement of DTH responses

Mice were tolerized by gavage with of 50 mg OVA (Grade III, Sigma-Aldrich) on 2 consecutive days. One week later, mice were immunized by subcutaneous injection between the shoulder blades of 300 μg OVA (Grade VI, Sigma Aldrich) in 200 μl PBS/Complete Freud's Adjuvant emulsion (Sigma-Aldrich). Two weeks after immunization, mice were challenged by subcutaneous injection of 50 μg OVA (Grade VI, Sigma Aldrich) in 20 μl PBS into the right ear pinna while 20 μl PBS without OVA were injected into the left ear pinna for control purposes. Ear thickness was measured in a blinded fashion prior to and 48 h after injection with a digital precision caliper. OVA-specific ear swelling was calculated as (right ear thickness - left ear thickness) at 48 h - (right ear thickness - left ear thickness) at 0 h.

Quantitative PCR

Sort-purified cells were lysed in Buffer RLT (QIAGEN). RNA was extracted via RNeasy mini kits (QIAGEN) as per the manufacturer's instructions. Reverse transcription of RNA was performed using Superscript reverse transcription according to the protocol provided by the manufacturer (Thermo Fisher Scientific). Real-time PCR was performed on cDNA using SYBR green chemistry (Applied Biosystems). Reactions were run on a real-time PCR system (ABI 7500; Applied Biosystems). Samples were normalized to *Hprt1* or *Gapdh* and displayed as a fold change as compared to controls.

ELISA

IL-2 in the supernatants was detected with a sandwich ELISA using anti-IL-2 clone JES6–1A12 as the capture antibody and anti-IL-2 clone JES-5H4 as the detection antibody (all from Thermo Fisher Scientific). The assay range of mouse IL-2 ELISA is from 15.6 to 1000 pg/ml and the analytical sensitivity is 5.3 pg/ml. For OVA-specific IgG1 quantification, 40 μg/ml OVA (Grade VI) was coated on an ELISA plate, mouse serum was diluted from $1:10^4$ to $1:10^6$, and an anti-OVA IgG1 (Cayman Chemical) standard curve ranging from 0.781 ng/ml to 100 ng/ml was applied. OVA-specific IgG1 was detected using an anti-mouse IgG1-HRP antibody (BD Biosciences). For fecal Lipocalin-2 detection, fecal samples were collected and weighted for data normalization, then were homogenized in PBS and centrifuged at 12,000 r.p.m. to remove aggregates, and the resulting supernatant was

collected. Afterwards, a sandwich ELISA was performed using Mouse Lipocalin-2/NGAL DuoSet ELISA (R&D Systems) according to the manufacturer's instructions.

Regulatory T cell suppression assay

DCs ($CD11c^+$ $MHCII^+$) or naive T cells ($CD3^+$ $CD4^+$ $CD25^-$ $CD45RB^{hi}$) were sort-purified from the spleen of WT or $Thy1.1^+$ mice, respectively. Small intestinal Tregs ($CD45^+$ $CD3^+$ $CD4^+$ $CD25^+$) were sort purified from either $Ncr1^{cre}$-$Il2^{f/f}$ mice or littermate controls and were subsequently found to be at least 95% $Foxp3^+$ T cells. DCs were plated at 4×10^3 per well in the presence of 1 μg/mL soluble purified anti-CD3 (clone 145–2C11, BD Biosciences). CFSE labelled T cells (2×10^4 per well) were mixed with Tregs at defined ratios and co-cultured with DCs in the presence of anti-CD3. After a 3-day culture, T cell proliferation was measured by CFSE dilution via flow cytometry. Treg suppression was calculated by gating on T effector cells and quantifying the percentage of CFSE-dilution in comparison to cells cultured in the absence of Tregs.

Histological staining

Tissue samples from the intestines of mice were fixed with 4% paraformaldehyde, embedded in paraffin, and 5 μm sections were stained with haematoxylin and eosin.

RNA-sequencing

ILC3 ($CD45^+CD3^-ROR\gamma t^{GFP+}CD127^+$) and $CD4^+$ T cells ($CD45^+CD3^+CD4^+$) were sort-purified from small intestine of $Rorc(\gamma t)$-Gfp^{TG} mice. Sorted cells were used to prepare RNA-seq libraries by the Epigenomics Core at Weill Cornell Medicine using the Clontech SMARTer Ultra Low Input RNA Kit V4 (Clontech Laboratories). Sequencing was performed on an Illumina HiSeq 2500, yielding 50 bp single-end reads. Raw sequencing reads were demultiplexed with Illumina CASAVA (v1.8.2). Adapters were trimmed from reads using FLEXBAR (v2.4) and reads were aligned to the NCBI GRCm38/mm10 mouse genome using the STAR aligner (v2.3.0) with default settings. Reads per gene were counted using Rsubread. One sample of the $CD4^+$ T cell group was removed, as its library size was anomalously small compared to those of the other samples. Genes with at least 10 counts in each sample were considered for further analysis. Differential expression was assessed using DESeq2 version 1.14.0 with default parameters and with a false discovery rate (FDR) of 0.1.

Statistical analysis

P value of mouse data sets was determined by paired or unpaired two-tailed Student's *t*-test with a 95% confidence interval. Variance was analyzed using F-test. Welch's correction was performed in case of unequal variance. Where appropriate, Mann-Whitney test, Wilcoxon matched-pairs test or two-way ANOVA followed by Bonferroni post-tests were performed. All statistical tests were performed with Graph Pad Prism V6 software. *P* values less than 0.05 were considered significant.

Extended Data

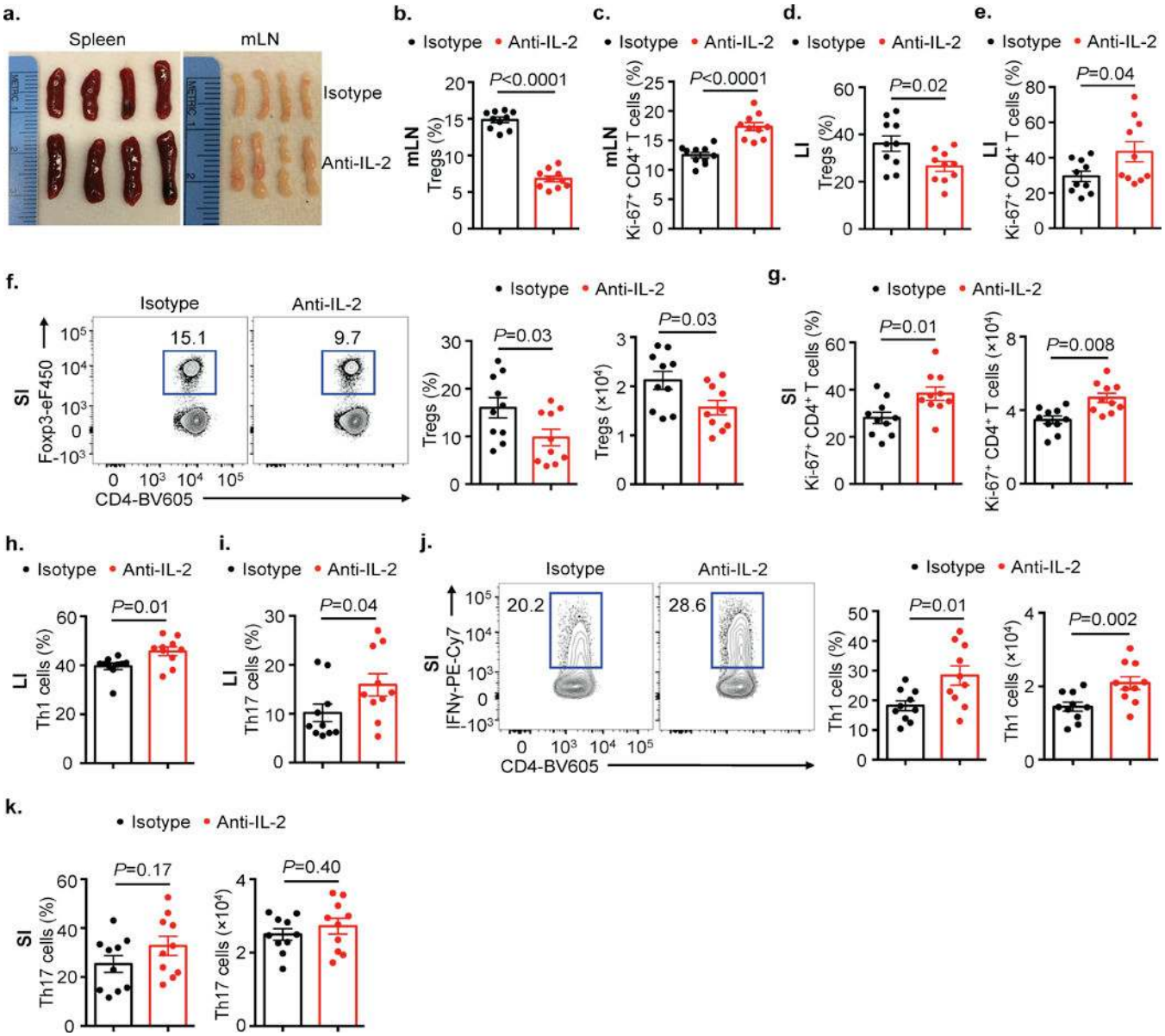

Extended Data Figure 1. IL-2 blockade results in disrupted T cell homeostasis throughout the intestinal tract and associated lymphoid tissues.

a-c, Sex- and age- matched C57BL/6 mice were treated with anti-IL-2 monoclonal antibodies every other day for two weeks and examined for the spleen and mesenteric lymph nodes (mLN) size (**a**), the frequency of Tregs (**b**) and Ki-67^{+}CD4^{+} T cells (**c**) of mLN by flow cytometry (n=10). **d**-**g**. Mice from **a-c** were also analyzed for the frequencies of Tregs (**d**) and Ki-67^{+}CD4^{+} T cells (**e**) in large intestine lamina propria cells (LI-LPs) and the frequencies and numbers of Tregs (**f**) and Ki-67^{+}CD4^{+} T cells (**g**) in small intestine lamina propria cells (SI-LPs) by flow cytometry (n=10). **h-k**. Mice from **a-c** were analyzed for the frequency of Th1 cells (**h**) and Th17 cells (**i**) in LI-LPs and the frequencies and numbers of Th1 cells (**j**) and Th17 cells (**k**) in SI-LPs by flow cytometry (n=10). Data in **a** are representative of two independent experiments with similar results. Data in **b-k** are pooled

from two independent experiments. Results are shown as the means ± s.e.m. All statistics are calculated by unpaired two-tailed Student's *t*-test. *P* values are indicated on the figure.

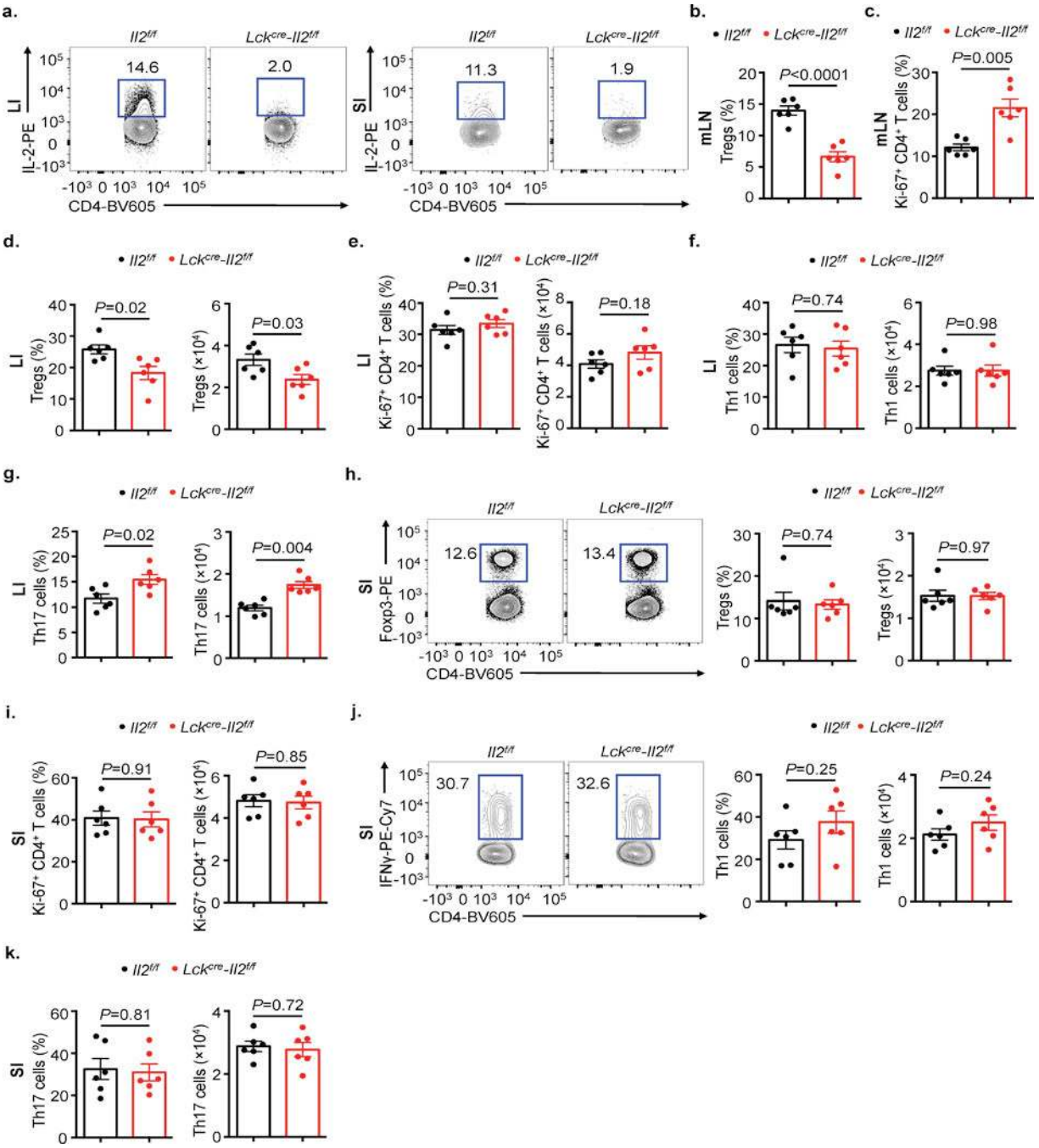

Extended Data Figure 2. T cell-derived IL-2 is essential for maintaining immunologic homeostasis in the mesenteric lymph node and large intestine.

a. Sex- and age- matched *Il2*$^{f/f}$ and *Lck*^{cre}-*Il2*$^{f/f}$ mice were examined for the deletion efficiency of IL-2 in CD4$^+$ T cells in the large and small intestines. **b**. Mice in **a** were examined for the frequency of Tregs (**b**) and Ki-67$^+$ CD4$^+$ T cells (**c**) from the mLN by flow cytometry (n=6). **d-g**. Mice in **a** were analyzed for the frequencies and numbers of Tregs (**d**), Ki-67$^+$ CD4$^+$ T cells (**e**), Th1 cells (**f**) and Th17 cells (**g**) of LI-LPs by flow cytometry (n=6). **h-k**. Mice in **a** were analyzed for the frequencies and numbers of Tregs (**h**), Ki-67$^+$ CD4$^+$ T

cells (**i**), Th1 cells (**j**) and Th17 cells (**k**) of SI-LPs by flow cytometry (n=6). Data in **a** is representative of two independent experiments with similar results. Data in **b-k** are pooled from two independent experiments. Results are shown as the means ± s.e.m. All statistics are calculated by unpaired two-tailed Student's *t*-test. *P* values are indicated on the figure.

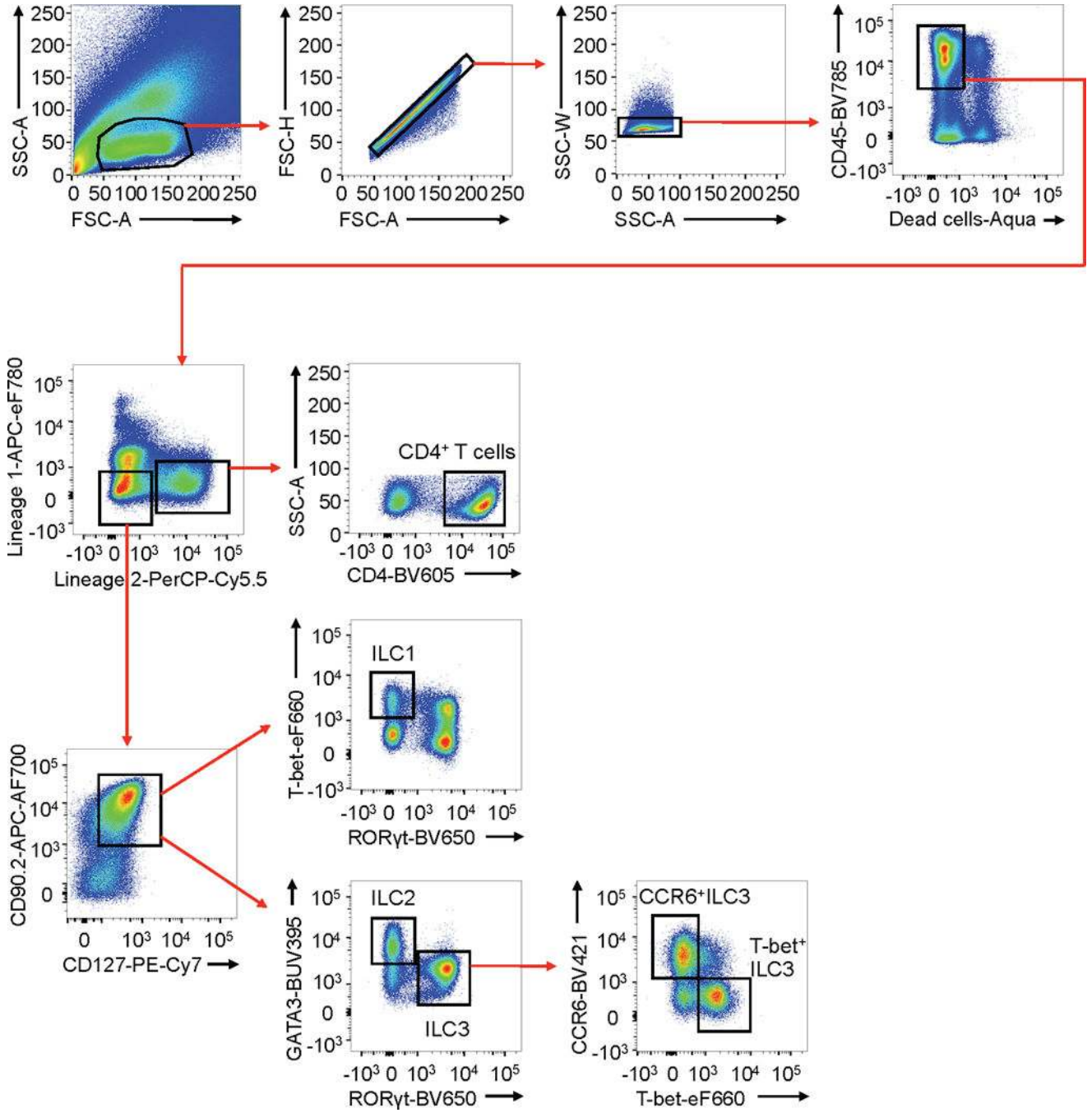

Extended Data Figure 3. Gating strategy to analyze innate lymphoid cells subsets and CD4$^+$ T cells in the small intestine.

Gating strategy for flow cytometry analysis of innate lymphoid cells and CD4$^+$ T cells in SI-LPs. Lineage 1: CD11b, CD11c and B220; lineage 2: CD3ε, CD5 and CD8α. CD4$^+$ T cells were identified as CD45$^+$Lineage 2$^+$ CD4$^+$, ILC1 were identified as CD45$^+$Lineage$^-$ CD127$^+$CD90.2$^+$T-bet$^+$RORγt$^-$, ILC2 were identified as CD45$^+$Lineage$^-$ CD127$^+$CD90.2$^+$GATA3$^+$, ILC3 were identified as CD45$^+$Lineage$^-$CD127$^+$CD90.2$^+$RORγt$^+$, ILC3 subsets were further identified as CCR6$^+$T-bet$^-$ ILC3 or CCR6$^-$T-bet$^+$ ILC3.

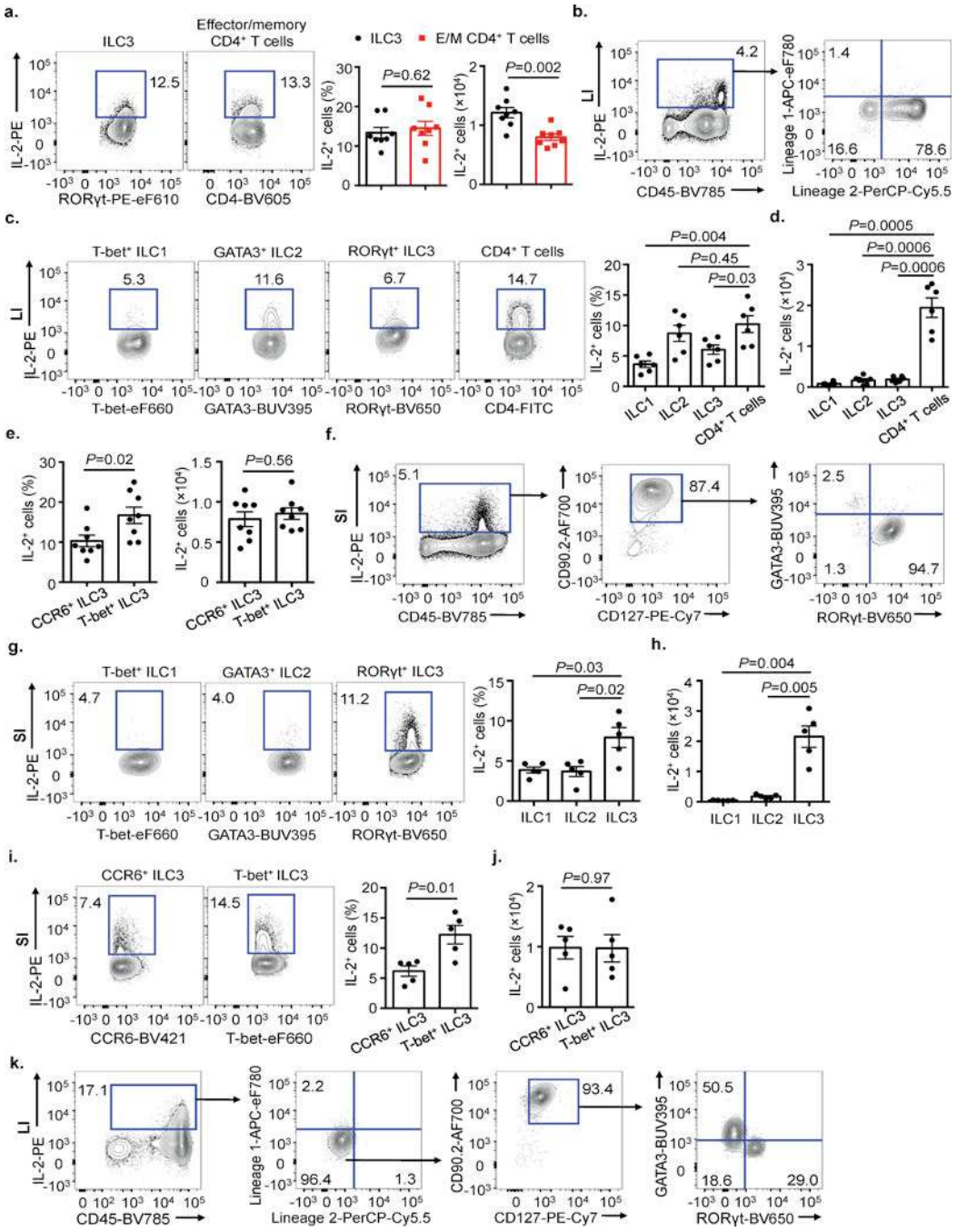

Extended Data Figure 4. IL-2$^+$ cells in the large intestine of WT mice and in the small and large intestines of *Rag1*$^{-/-}$ mice.

a. Flow cytometry plots with graph of frequency and numbers of IL-2 in ILC3 and Effector/memory (E/M) CD4$^+$ T cells (CD3$^+$CD4$^+$Foxp3$^-$CD44^{hi}CD62L^{lo}) in SI-LPs of WT mice (n=8). **b**. Flow cytometry plots show IL-2$^+$ cells in LI-LPs of C57BL/6 mice. Lineage 1: CD11b, CD11c and B220; lineage 2: CD3ε, CD5 and CD8α. **c**, **d**. Flow cytometry plots with graph of frequency (**c**) and absolute numbers (**d**) of IL-2$^+$ cells in LI-LPs of C57BL/6 mice (n=6). **e**. The frequency and number of IL-2$^+$ ILC3 subsets in SI-LPs of C57BL/6 mice

(n=8). **f**. Flow cytometry plots show IL-2$^+$ cells in SI-LPs of *Rag1*$^{-/-}$ mice. **g**, **h**. Flow cytometry plots with graph of frequency (**g**) and absolute numbers (**h**) of IL-2$^+$ cells in SI-LPs of *Rag1*$^{-/-}$ mice (n=5). **i**, **j**. Flow cytometry plots with graph of frequency (**i**) and absolute numbers (**j**) of IL-2$^+$ ILC3 subsets in SI-LPs of *Rag1*$^{-/-}$ mice (n=5). **k**. Flow cytometry plots show IL-2$^+$ cells in LI-LPs of *Rag1*$^{-/-}$ mice. Lineage 1: CD11b, CD11c and B220; lineage 2: CD3ε, CD5 and CD8α. Data in **b** and **f-k** are representative of two independent experiments with similar results. Data in **a** and **c-e** are pooled from two independent experiments. Results are shown as the means ± s.e.m. Statistics are calculated by paired or unpaired two-tailed Student's *t*-test. *P* values are indicated on the figure.

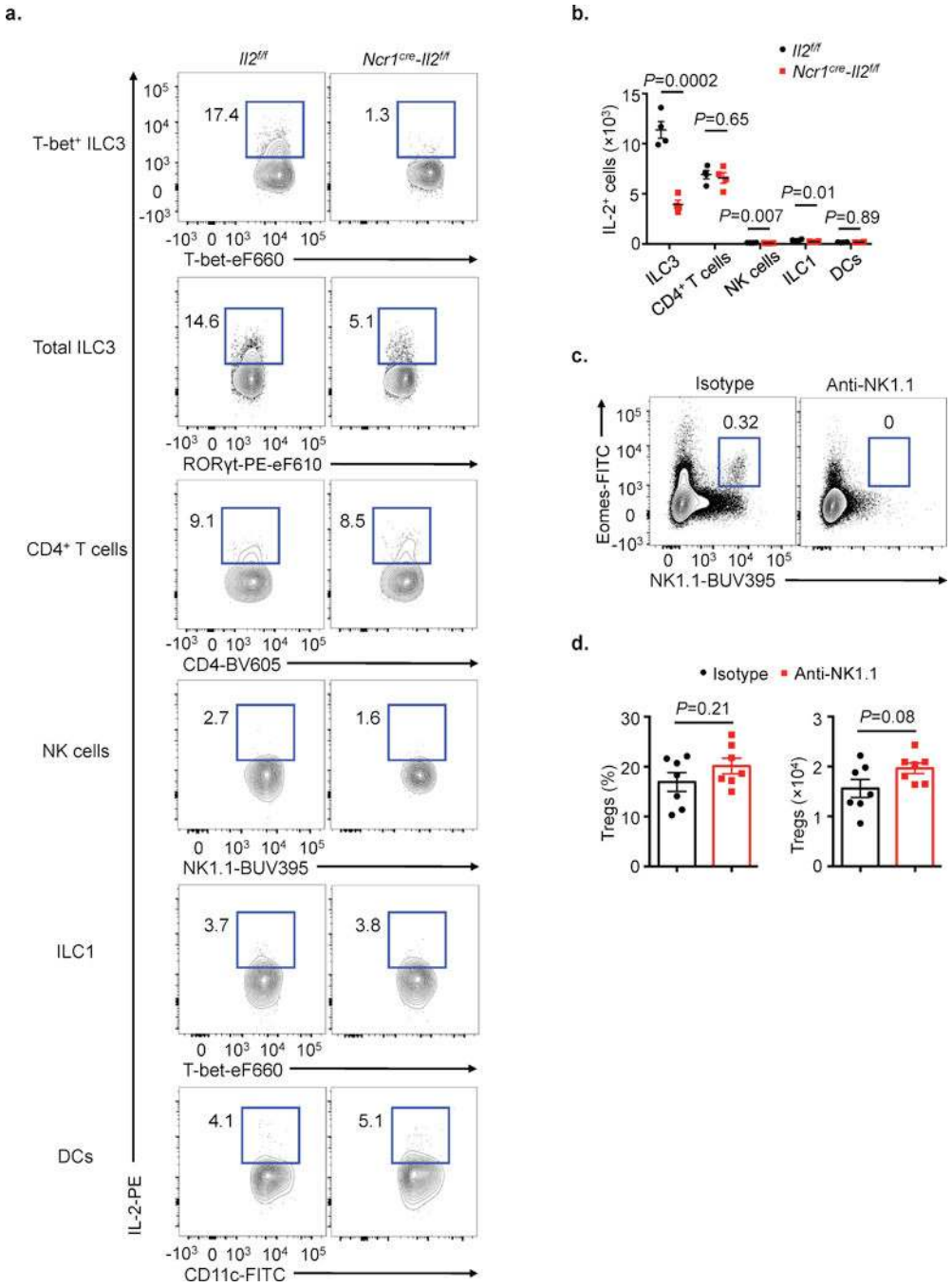

Extended Data Figure 5. NK cells and ILC1 are dispensable for maintenance of Tregs in small intestine.

a. IL-2 was assessed in T-bet$^+$ ILC3, total ILC3, CD4$^+$ T cells, NK cells, ILC1 and DCs in SI-LPs of *Il2*$^{f/f}$ and *Ncr1*^{cre}-*Il2*$^{f/f}$ mice. **b**. The number of IL-2$^+$ cells were quantified in SI-LPs of *Il2*$^{f/f}$ and *Ncr1*^{cre}-*Il2*$^{f/f}$ mice (n=4). **c**, **d**. Sex- and age- matched C57BL/6 mice were treated with anti-NK1.1 monoclonal antibody every 3 days for two weeks and examined for NK cell depletion efficiency (**c**) and the frequency and number of Tregs in SI-LPs (**d**) (n=7). Data in **a-c** are representative of two independent experiments with similar results. Data in **d**

is pooled from two independent experiments. Results are shown as the means ± s.e.m. Statistics are calculated by unpaired two-tailed Student's *t*-test. *P* values are indicated on the figure.

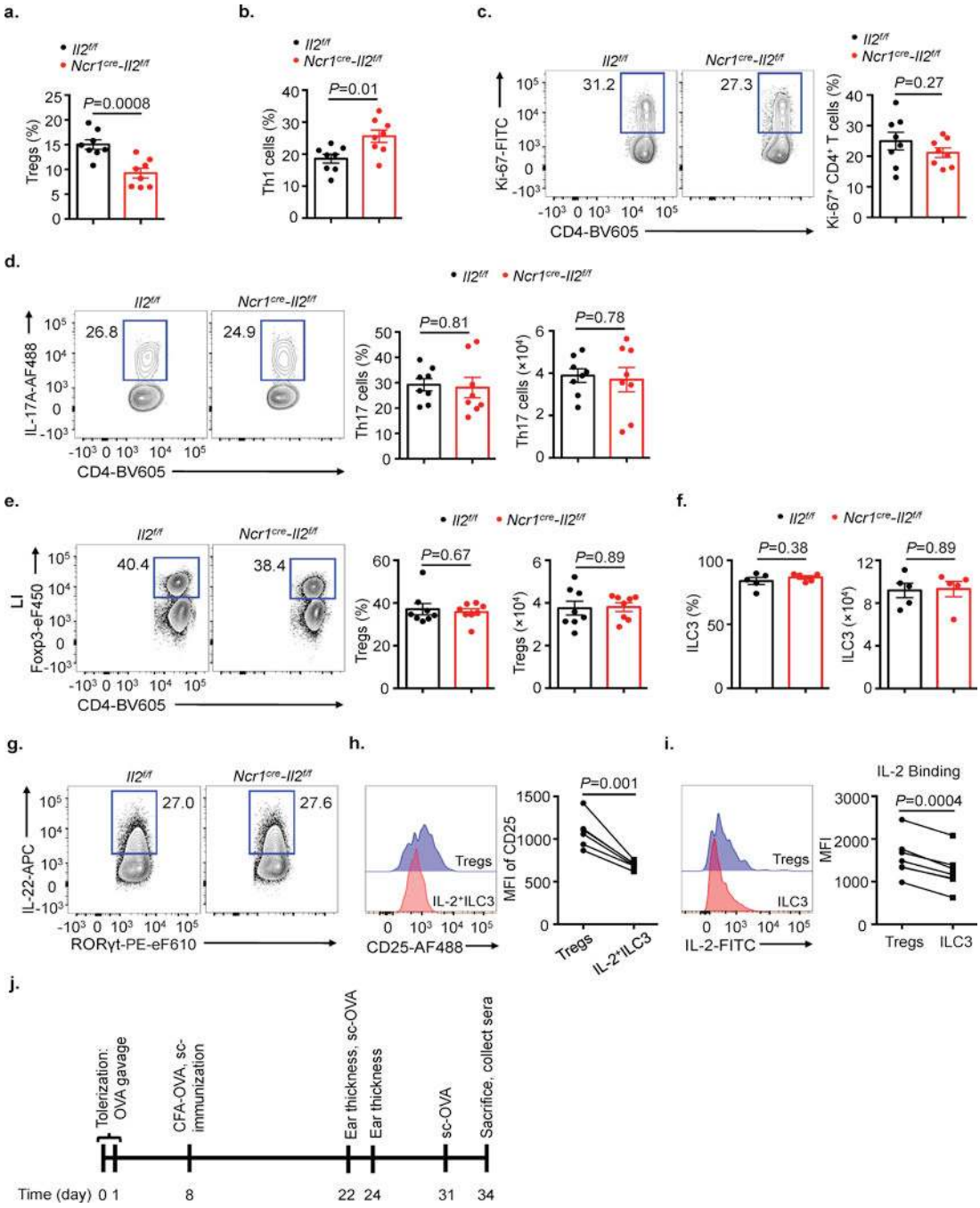

Extended Data Figure 6. ILC3-derived IL-2 is dispensable for the maintenance of small intestinal Th17 cells, ILC3 homeostasis and large intestinal Tregs.

a-d. *Il2*$^{f/f}$ and *Ncr1*^{cre}-*Il2*$^{f/f}$ mice were analyzed for the percentage of Tregs (**a**), Th1 cells (**b**), Ki-67^{+} CD4^{+} T cells (**c**) and the frequency and cell number of Th17 cells (**d**) in SI-LPs at steady state by flow cytometry (n=8). **e**. *Il2*$^{f/f}$ and *Ncr1*^{cre}-*Il2*$^{f/f}$ mice were examined for the frequency and number of Tregs in LI-LPs by flow cytometry (n=8). **f.** *Il2*$^{f/f}$ and *Ncr1*^{cre}-*Il2*$^{f/f}$ mice were examined for the frequency and number of ILC3 in SI-LPs by flow cytometry (n=8). **g**. IL-22 was assessed in ILC3 from SI-LPs of *Il2*$^{f/f}$ or *Ncr1*^{cre}-*Il2*$^{f/f}$ mice.

h. Representative histograms and bar graph examination of CD25 staining on Tregs and IL-2^{+} ILC3. **i**. Representative histograms demonstrating IL-2 binding capacity and quantification of bound IL-2 MFI in Tregs and ILC3. **j.** Experimental design of the DTH model. Data in **f-h** are representative of two independent experiments with similar results (at least 3 mice per group). Data in **a-e** and **i** are pooled from two independent experiments. Results are shown as the means ± s.e.m. Statistics are calculated by paired or unpaired two-tailed Student's *t*-test. *P* values are indicated on the figure.

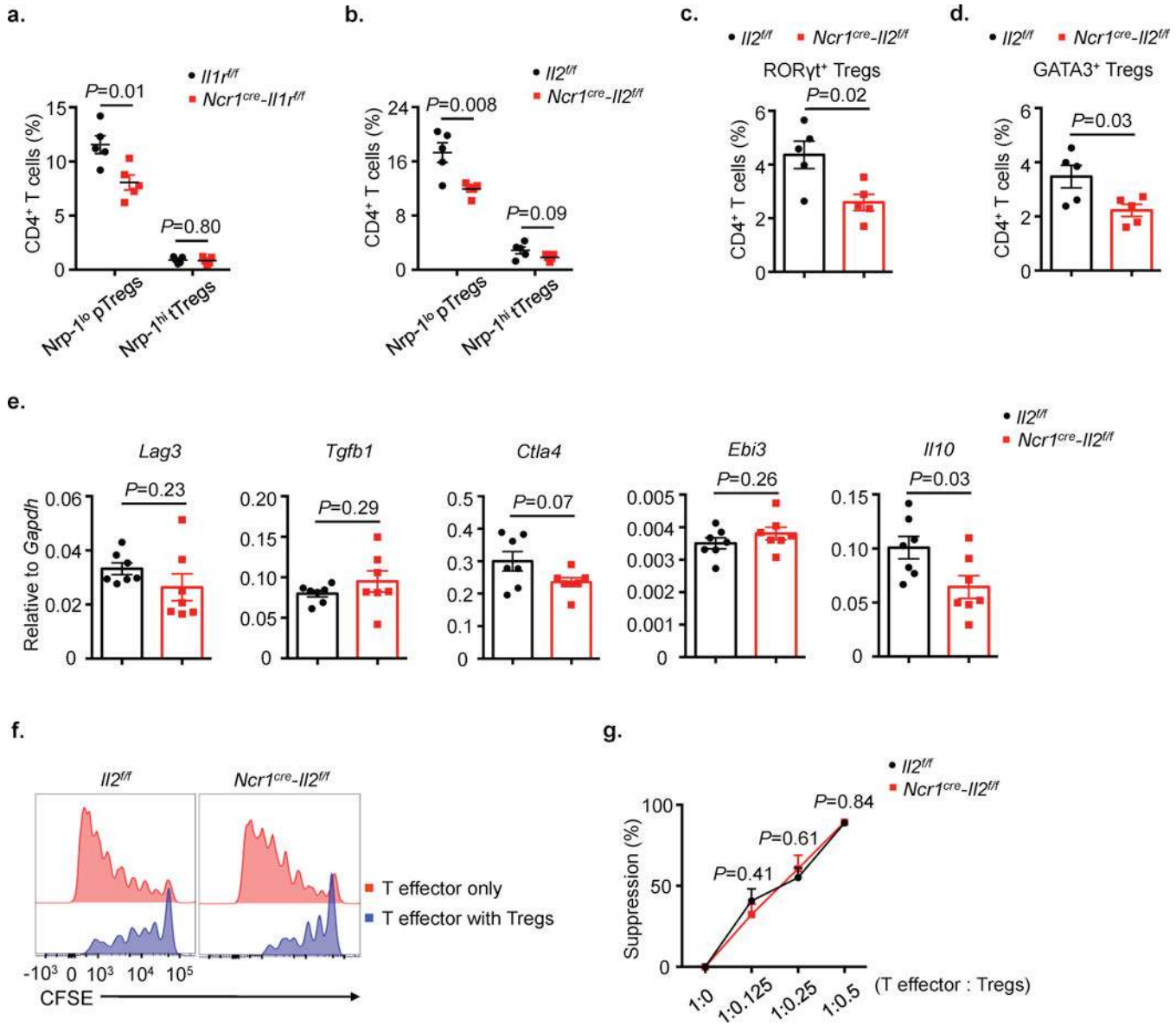

Extended Data Figure 7. Deletion of ILC3-intrinsic IL-2 affects the population size of peripherally-induced Tregs, but not their suppressive capacity.

a, **b**. The frequency of peripheral Tregs (Nrp-1^{lo} pTregs) and Thymic Tregs (Nrp-1^{hi} tTregs) were characterized in SI-LPs of *Il1r*$^{f/f}$ and *Ncr1*^{cre}-*Il1r*$^{f/f}$ mice (**a**) or *Il2*$^{f/f}$ and *Ncr1*^{cre}-*Il2*$^{f/f}$ mice (**b**) (n=5). **c**, **d**. The frequency of Treg subsets were analyzed in SI-LPs of *Il2*$^{f/f}$ and *Ncr1*^{cre}-*Il2*$^{f/f}$ mice (n=5). **e**. Small intestinal Tregs were examined for expression of *Lag3*, *Tgfb1*, *Ctla4*, *Ebi3* and *Il10* in *Il2*$^{f/f}$ and *Ncr1*^{cre}-*Il2*$^{f/f}$ mice (n=7). **f**, **g**. Sort-purified small intestinal CD45$^+$CD3$^+$CD4$^+$CD25$^+$ regulatory T cells were co-cultured with sort-purified CFSE-labeled splenic effector T cells (CD3$^+$CD4$^+$CD25$^-$CD45RB^{hi}) in the presence of purified splenic DCs and soluble anti-CD3 for 3 days. CFSE dilution was analyzed and quantified (n=6). Data in **a-d** and **f** are representative of two independent experiments with similar results. Data in **e** and **g** are pooled from two independent experiments. Results are

shown as the means ± s.e.m. Statistics are calculated by unpaired two-tailed Student's *t*-test. *P* values are indicated on the figure.

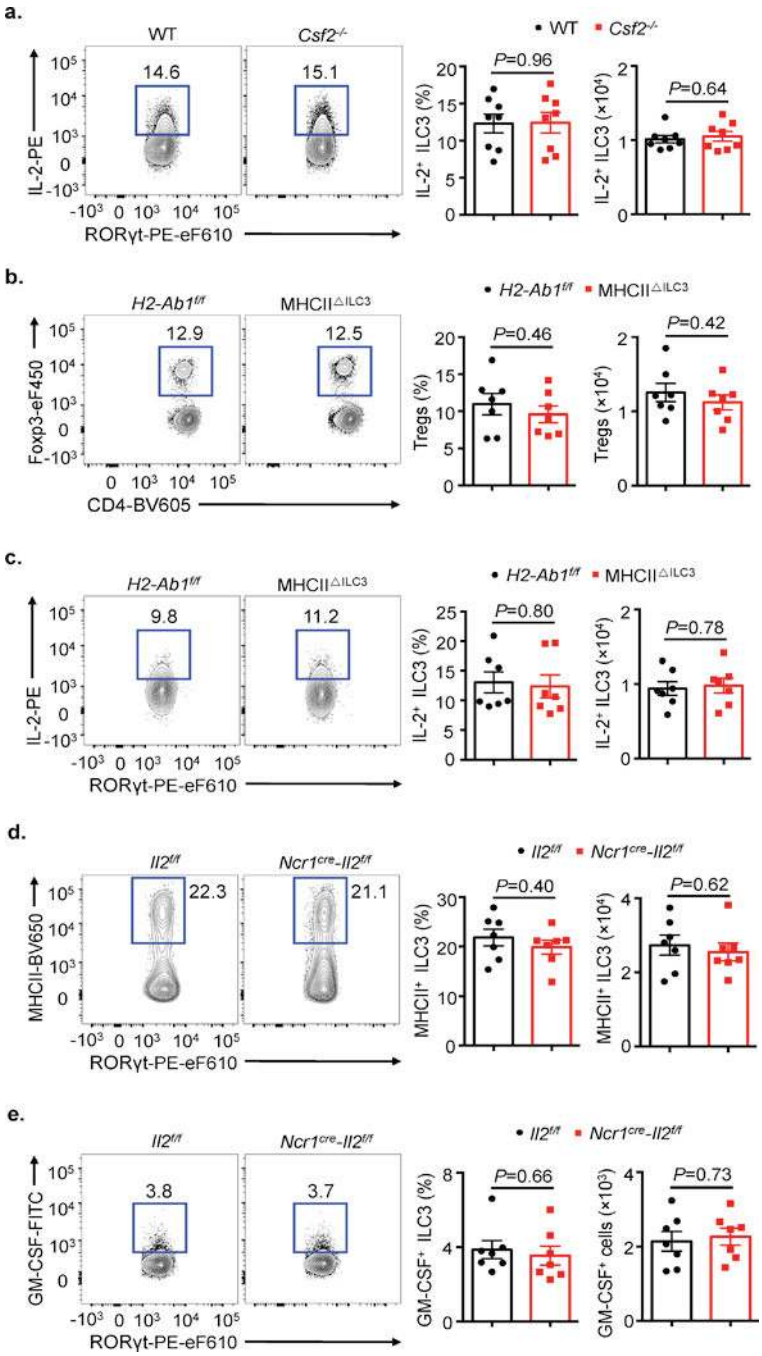

Extended Data Figure 8. ILC3-derived IL-2 does not exhibit functional redundancy or hierarchies with ILC3-specific GM-CSF or MHCII.

a. Flow cytometry plots with graph of frequency and quantification of cell numbers of IL-2$^+$ ILC3 in SI-LPs of WT and *Csf2*$^{-/-}$ mice (n=8). **b**, **c**. Flow cytometry plots with graph of frequency and quantification of cell numbers of Tregs (**b**) and IL-2$^+$ ILC3 (**c**) in SI-LPs of *H2-Ab1*$^{f/f}$ and MHCII$^{\Delta ILC3}$ mice (n=7). **d**, **e**. Flow cytometry plots with graph of frequency and quantification of cell numbers of MHCII$^+$ ILC3 (**d**) and GM-CSF$^+$ ILC3 (**e**) in SI-LPs of *Il2*$^{f/f}$ and *Ncr1*^{cre}-*Il2*$^{f/f}$ mice (n=7). Data are pooled from two independent experiments.

Results are shown as the means ± s.e.m. Statistics are calculated by unpaired two-tailed Student's *t*-test. *P* values are indicated on the figure.

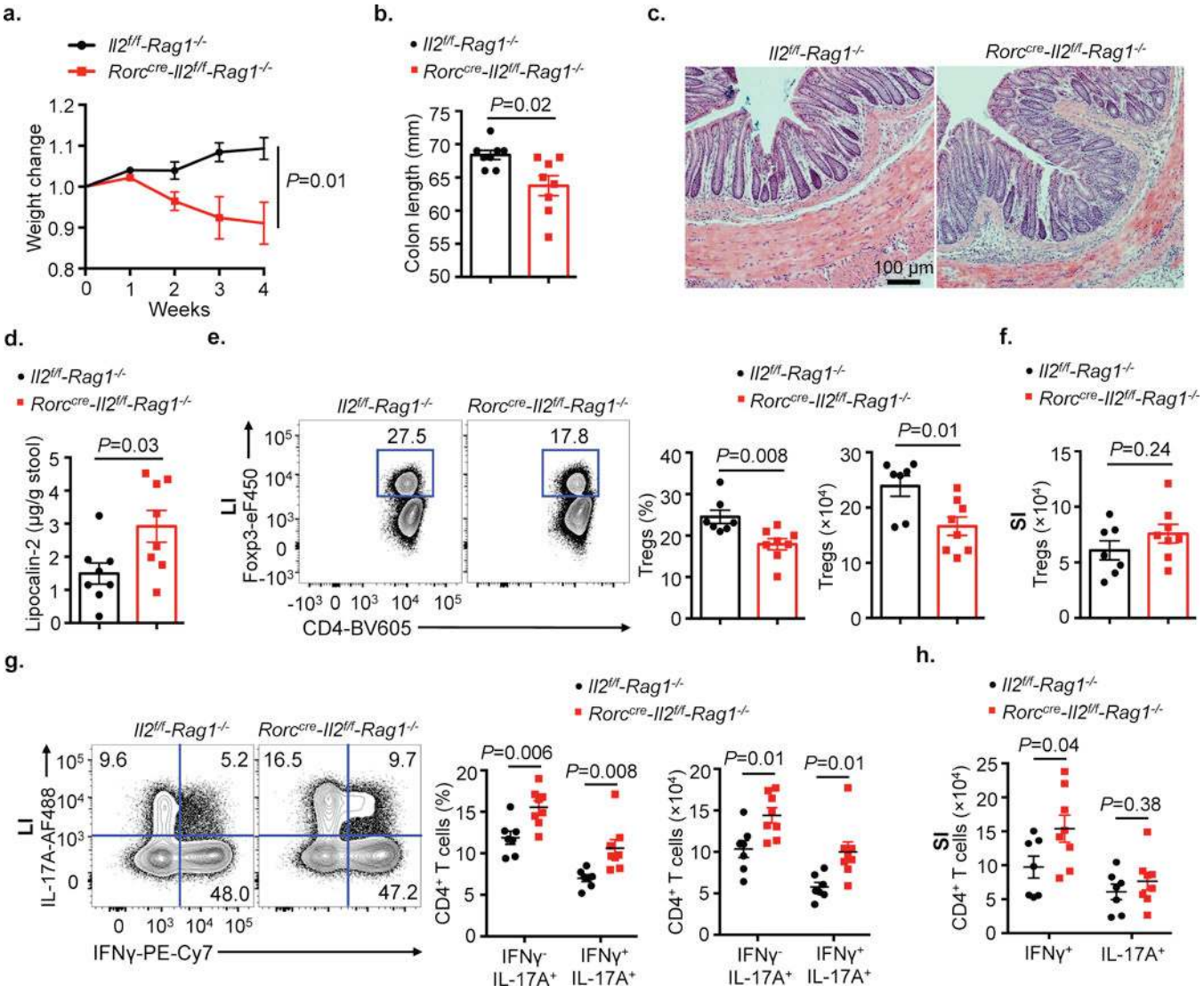

Extended Data Figure 9. ILC3-derived IL-2 promotes essential immune regulation in the intestine.

a-h. CD4$^+$ T cells were adoptively transferred into *Il2$^{f/f}$-Rag1$^{-/-}$* or *Rorc^{cre}-Il2$^{f/f}$-Rag1$^{-/-}$* recipient mice. Recipients were examined for changes in weight (**a**), colon length (**b**), histological H&E staining in the terminal colon (**c**) and Lipocalin-2 presence in fecal samples (**d**) (n=8). **e**. Flow cytometry plots with graph of percentage and absolute cell number of Tregs in LI-LPs in defined recipients. **f.** Absolute cell number of Tregs in SI-LPs in defined recipients. **g**. Flow cytometry plots and graph of frequency and absolute number of IFNγ^-IL-17A$^+$ and IFNγ^+IL-17A$^+$ cells in LI-LPs in defined recipients. **h**. Cell number of Th1 and Th17 cells in SI-LPs in defined recipients. N=7 of *Il2$^{f/f}$-Rag1$^{-/-}$* group and n=8 of *Rorc^{cre}-Il2$^{f/f}$-Rag1$^{-/-}$* group are the details of mice in **e-h**. Data in **a-h** are pooled from two independent experiments. Results are shown as the means ± s.e.m. Statistics are calculated by unpaired two-tailed Student's *t*-test. *P* values are indicated on the figure.

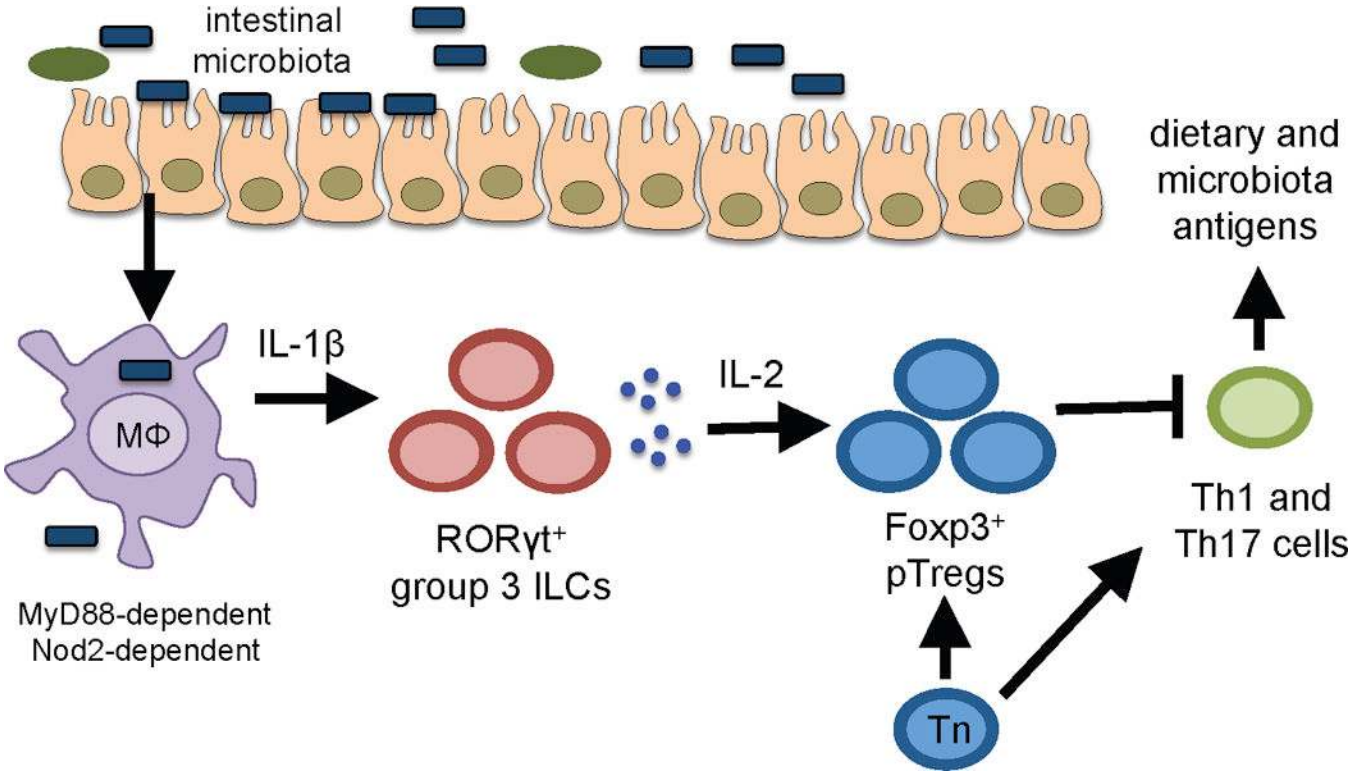

Extended Data Figure 10. A novel IL-1β-ILC3-IL-2 circuit is essential for the maintenance of Tregs and immunologic homeostasis uniquely within the small intestine.

In this manuscript we define a novel pathway of immune regulation in the small intestine. This pathway is continuously required and involves MyD88- and Nod2-dependent microbial sensing by macrophages, production of IL-1β and induction of ILC3-derived IL-2 to support the maintenance of peripherally-induced intestinal Tregs. Consequently, this is essential to maintain immunologic homeostasis and oral tolerance, and becomes dysregulated in human IBD.

Acknowledgements

We thank members of the Sonnenberg Laboratory for discussions and critical reading of the manuscript. We also thank Drs. Tatsuichiro Shima and Yoshinori Umesaki from Yakult Central Institute (Tokyo, Japan) for providing SFB and important advice. Research in the Sonnenberg Laboratory is supported by the National Institutes of Health (R01AI143842, R01AI123368, R01AI145989, R21DK110262 and U01AI095608), the NIAID Mucosal Immunology Studies Team (MIST), the Crohn's and Colitis Foundation of America, the Searle Scholars Program, the American Asthma Foundation Scholar Award, Pilot Project Funding from the Center for Advanced Digestive Care (CADC), an Investigators in the Pathogenesis of Infectious Disease Award from the Burroughs Wellcome Fund, a Wade F.B. Thompson/Cancer Research Institute CLIP Investigator grant, the Meyer Cancer Center Collaborative Research Initiative, and the Jill Roberts Institute (JRI) for Research in IBD. L.Z. and J.G. are supported by fellowships from the Crohn's and Colitis Foundation (608975 and 519428). N.J.B. is supported by a fellowship from the NIH (F32AI124517). We would like to thank the Epigenomics Core of Weill Cornell Medicine. We would like to thank all contributing members of the JRI IBD Live Cell Bank, which is supported by the JRI, Jill Roberts Center for IBD, Cure for IBD, the Rosanne H. Silbermann Foundation and Weill Cornell Medicine Division of Pediatric Gastroenterology and Nutrition. Research in the Vivier lab is supported by funding form the European Research Council (ERC) under the European Union's Horizon 2020 research and innovation programme (TILC, grant agreement N°694502); the Agence Nationale de la Recherche; Equipe Labellisée "La Ligue," Ligue Nationale contre le Cancer, MSDAvenir, Innate Pharma and institutional grants to the CIML (INSERM, CNRS, and Aix-Marseille University) and to Marseille Immunopôle.

References

1. Boyman O & Sprent J The role of interleukin-2 during homeostasis and activation of the immune system. Nature reviews. Immunology 12, 180–190, 10.1038/nri3156 (2012).
2. Malek TR The biology of interleukin-2. Annual review of immunology 26, 453–479, 10.1146/annurev.immunol.26.021607.090357 (2008).
3. Sadlack B et al. Ulcerative colitis-like disease in mice with a disrupted interleukin-2 gene. Cell 75, 253–261 (1993). [PubMed: 8402910]
4. Josefowicz SZ, Lu LF & Rudensky AY Regulatory T cells: mechanisms of differentiation and function. Annu Rev Immunol 30, 531–564, 10.1146/annurev.immunol.25.022106.141623 (2012). [PubMed: 22224781]
5. Belkaid Y & Tarbell K Regulatory T cells in the control of host-microorganism interactions (*). Annual review of immunology 27, 551–589, 10.1146/annurev.immunol.021908.132723 (2009).
6. Izcue A, Coombes JL & Powrie F Regulatory lymphocytes and intestinal inflammation. Annual review of immunology 27, 313–338, 10.1146/annurev.immunol.021908.132657 (2009).
7. Tanoue T, Atarashi K & Honda K Development and maintenance of intestinal regulatory T cells. Nature reviews. Immunology 16, 295–309, 10.1038/nri.2016.36 (2016).
8. Zhou L & Sonnenberg GF Essential immunologic orchestrators of intestinal homeostasis. Science immunology 3, 10.1126/sciimmunol.aao1605 (2018).
9. Klatzmann D & Abbas AK The promise of low-dose interleukin-2 therapy for autoimmune and inflammatory diseases. Nat Rev Immunol 15, 283–294, 10.1038/nri3823 (2015). [PubMed: 25882245]
10. Popmihajlov Z, Xu D, Morgan H, Milligan Z & Smith KA Conditional IL-2 Gene Deletion: Consequences for T Cell Proliferation. Front Immunol 3, 102, 10.3389/fimmu.2012.00102 (2012). [PubMed: 22590468]
11. Artis D & Spits H The biology of innate lymphoid cells. Nature 517, 293–301, 10.1038/nature14189 (2015). [PubMed: 25592534]
12. Spits H et al. Innate lymphoid cells--a proposal for uniform nomenclature. Nat Rev Immunol 13, 145–149 (2013). [PubMed: 23348417]
13. Sonnenberg GF & Artis D Innate lymphoid cells in the initiation, regulation and resolution of inflammation. Nat Med 21, 698–708, 10.1038/nm.3892[pii] (2015). [PubMed: 26121198]
14. Atarashi K et al. Th17 Cell Induction by Adhesion of Microbes to Intestinal Epithelial Cells. Cell 163, 367–380, 10.1016/j.cell.2015.08.058 (2015). [PubMed: 26411289]
15. Gaboriau-Routhiau V et al. The key role of segmented filamentous bacteria in the coordinated maturation of gut helper T cell responses. Immunity 31, 677–689, 10.1016/j.immuni.2009.08.020 (2009). [PubMed: 19833089]
16. Sano T et al. An IL-23R/IL-22 Circuit Regulates Epithelial Serum Amyloid A to Promote Local Effector Th17 Responses. Cell 164, 324, 10.1016/j.cell.2015.12.047 (2016). [PubMed: 28915371]
17. Philpott DJ, Sorbara MT, Robertson SJ, Croitoru K & Girardin SE NOD proteins: regulators of inflammation in health and disease. Nat Rev Immunol 14, 9–23, 10.1038/nri3565 (2014). [PubMed: 24336102]
18. Narni-Mancinelli E et al. Fate mapping analysis of lymphoid cells expressing the NKp46 cell surface receptor. Proc Natl Acad Sci U S A 108, 18324–18329, 10.1073/pnas.1112064108 (2011). [PubMed: 22021440]
19. Robson MJ et al. Generation and Characterization of Mice Expressing a Conditional Allele of the Interleukin-1 Receptor Type 1. PLoS One 11, e0150068, 10.1371/journal.pone.0150068 (2016). [PubMed: 26930558]
20. Mortha A et al. Microbiota-dependent crosstalk between macrophages and ILC3 promotes intestinal homeostasis. Science 343, 1249288, 10.1126/science.1249288 [pii] (2014). [PubMed: 24625929]
21. Hepworth MR et al. Innate lymphoid cells regulate CD4+ T-cell responses to intestinal commensal bacteria. Nature 498, 113–117 (2013). [PubMed: 23698371]

22. Hepworth MR et al. Immune tolerance. Group 3 innate lymphoid cells mediate intestinal selection of commensal bacteria-specific CD4(+) T cells. Science 348, 1031–1035, 10.1126/science.aaa4812 (2015). [PubMed: 25908663]

23. Kim KS et al. Dietary antigens limit mucosal immunity by inducing regulatory T cells in the small intestine. Science 351, 858–863, 10.1126/science.aac5560 (2016). [PubMed: 26822607]

24. Hadis U et al. Intestinal tolerance requires gut homing and expansion of FoxP3+ regulatory T cells in the lamina propria. Immunity 34, 237–246, 10.1016/j.immuni.2011.01.016 (2011). [PubMed: 21333554]

25. Pabst O & Mowat AM Oral tolerance to food protein. Mucosal Immunol 5, 232–239, 10.1038/mi.2012.4 (2012). [PubMed: 22318493]

26. Boschetti G et al. Therapy with anti-TNFalpha antibody enhances number and function of Foxp3(+) regulatory T cells in inflammatory bowel diseases. Inflammatory bowel diseases 17, 160–170, 10.1002/ibd.21308 (2011). [PubMed: 20848510]

27. Bernink JH et al. Human type 1 innate lymphoid cells accumulate in inflamed mucosal tissues. Nat Immunol 14, 221–229 (2013). [PubMed: 23334791]

28. Johansson ME & Hansson GC Immunological aspects of intestinal mucus and mucins. Nat Rev Immunol 16, 639–649, 10.1038/nri.2016.88 (2016). [PubMed: 27498766]

29. Mowat AM & Agace WW Regional specialization within the intestinal immune system. Nat Rev Immunol 14, 667–685, 10.1038/nri3738 (2014). [PubMed: 25234148]

30. Maloy KJ & Powrie F Intestinal homeostasis and its breakdown in inflammatory bowel disease. Nature 474, 298–306, 10.1038/nature10208 [pii] (2011). [PubMed: 21677746]

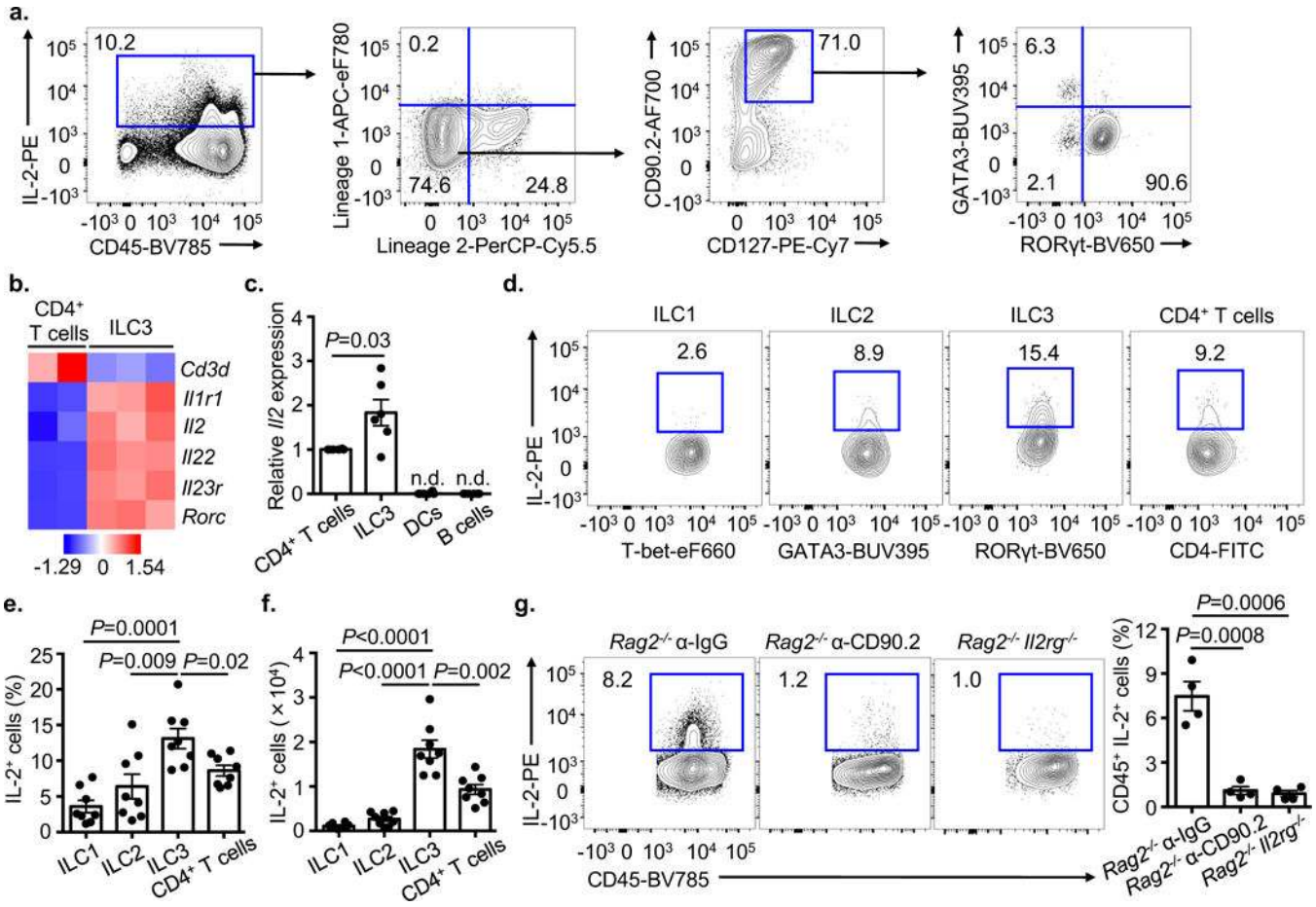

Figure 1. IL-2 is dominantly produced by ILC3 in the small intestine.

a. Flow cytometry plots show IL-2 staining in cells from the SI-LPs of C57BL/6 mice. Lineage 1: CD11b, CD11c and B220; lineage 2: CD3ε, CD5 and CD8α. **b**. Heatmap showing expression Z-scores of the indicated genes in CD4$^+$ T cells (CD45$^+$CD3$^+$CD4$^+$) and ILC3 (CD45$^+$CD3$^-$RORγt^{GFP+}CD127$^+$) from SI-LPs of *Rorc(γt)-Gfp^{TG}* mice, as measured by RNA-seq. **c**. Transcription of *Il2* in the sort-purified CD4$^+$ T cells, ILC3, DCs (CD45$^+$CD11c^{hi}MHCII$^+$CD64$^-$) and B cells (CD45$^+$CD19$^+$) from SI-LPs of *Rorc(γt)-Gfp^{TG}* mice, as determined by qPCR analysis (n=6). *Il2* expression was normalized to *Hprt1*, then further normalized to the CD4$^+$ T cells within each mouse. n.d., not detectable. **d-f**. Flow cytometry plots (**d**), graph of frequency (**e**) and quantification of cell number (**f**) of IL-2$^+$ cells in SI-LPs of C57BL/6 mice (n=8). **g**. Flow cytometry plots show IL-2 staining in SI-LPs from noted mice. Bar graph shows percentages in each group of mice (n=4). Data in **c, e** and **f** are pooled from two independent experiments. Data in **a** or **g** are representative of four or two independent experiments with similar results, respectively, at least 3 mice per group. Results are shown as the means ± s.e.m. Statistics are calculated by paired or unpaired two-tailed Student's *t*-test. *P* values are indicated on the figure.

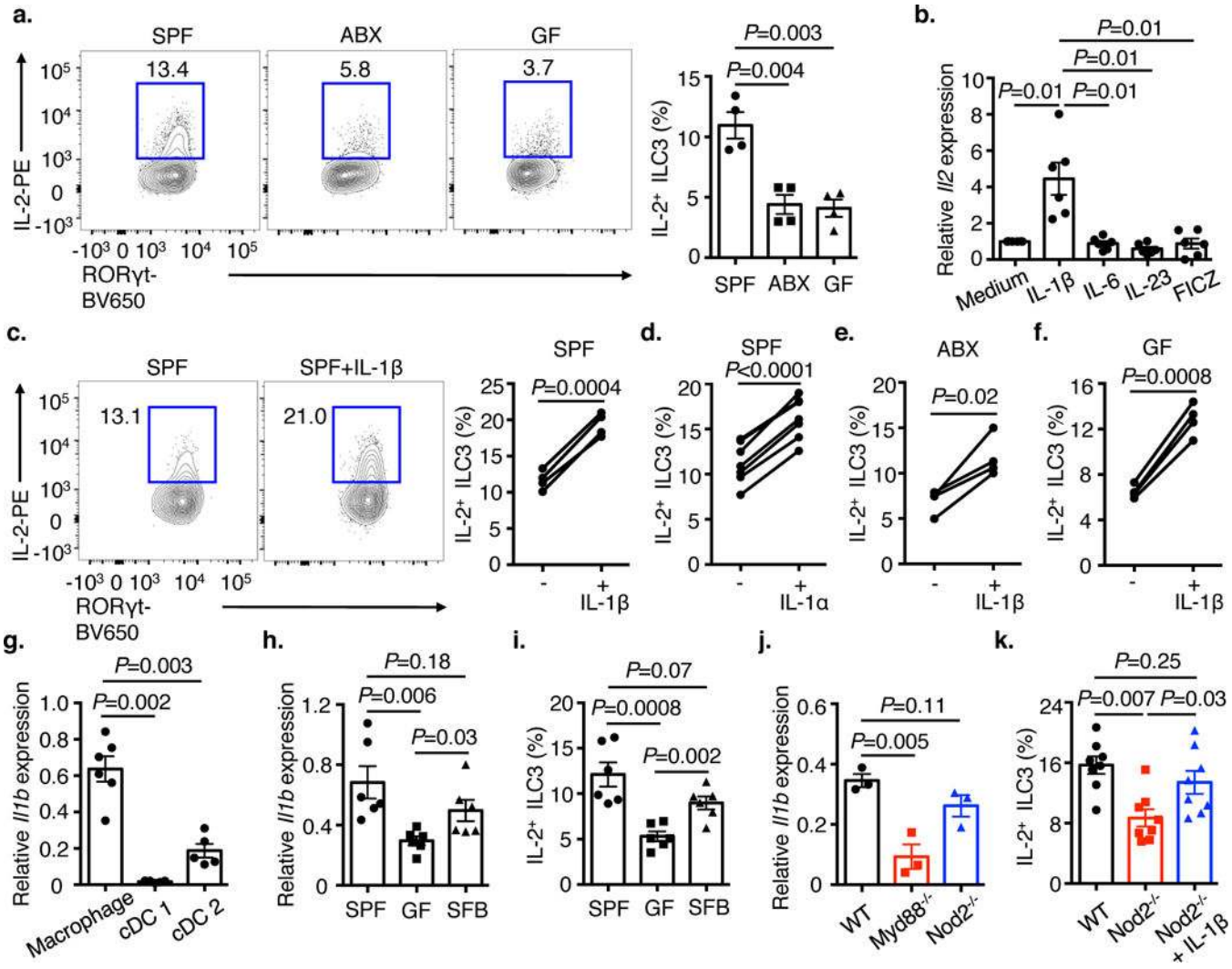

Figure 2. Sensing of the microbiota and production of IL-1β induces ILC3-derived IL-2.

a. Flow cytometry plots with graph of frequency of IL-2$^+$ ILC3 in SI-LPs of conventional (SPF), antibiotics treated (ABX) and germ free (GF) mice (n=4). **b**. qPCR examination of *Il2* transcript in sort-purified ILC3 in the presence of various stimulus (n=6). *Il2* expression was normalized to *Hprt1*, then further normalized to the medium control within each mouse. **c**. Flow cytometry plots with graph of frequency of IL-2$^+$ ILC3 from the SI-LPs of SPF mice following *ex vivo* culture (n=4). **d**. SI-LPs from SPF mice were cultured *ex vivo* for 4h with or without IL-1α and examined for IL-2$^+$ ILC3 by flow cytometry (n=7). **e**, **f**. SI-LPs from ABX (**e**) or GF (**f**) mice were cultured *ex vivo* with or without IL-1β and examined for IL-2 in ILC3 by flow cytometry (n=4). **g**. qPCR analysis of *Il1b* transcript in sort-purified macrophages (CD45$^+$CD11b$^+$CD64$^+$F4/80$^+$), conventional DC1 (cDC1) (CD45$^+$CD11c$^+$MHCII$^+$CD64$^-$XCR1$^+$CD172a$^-$) and cDC2 (CD45$^+$CD11c$^+$MHCII$^+$CD64$^-$XCR1$^-$CD172a$^+$) in SI-LPs (n=6). *Il1b* expression was normalized to *Gapdh*. **h**, **i**. qPCR analysis of *Il1b* transcript in sort-purified small intestinal macrophages (**h**) or flow cytometry analysis of ILC3-derived IL-2 expression (**i**) in SPF, GF and SFB mono-colonized mice (n=6). **j**. qPCR analysis of *Il1b* transcript in sort-purified small intestinal macrophages in wild-type (WT),

Myd88$^{-/-}$ and *Nod2*$^{-/-}$ mice (n=3). **k**. Flow cytometry analysis of small intestinal IL-2^{+} ILC3 in WT, *Nod2*$^{-/-}$ mice and *Nod2*$^{-/-}$ mice following *ex vivo* culture (n=8). Data in **a**, **c**, **e**, **f** and **j** are representative of two or three independent experiments with similar results (at least 3 mice per group). Data in **b**, **d**, **g-i** and **k** are pooled from two independent experiments. Results are shown as the means ± s.e.m. Statistics are calculated by paired or unpaired two-tailed Student's *t*-test. *P* values are indicated on the figure.

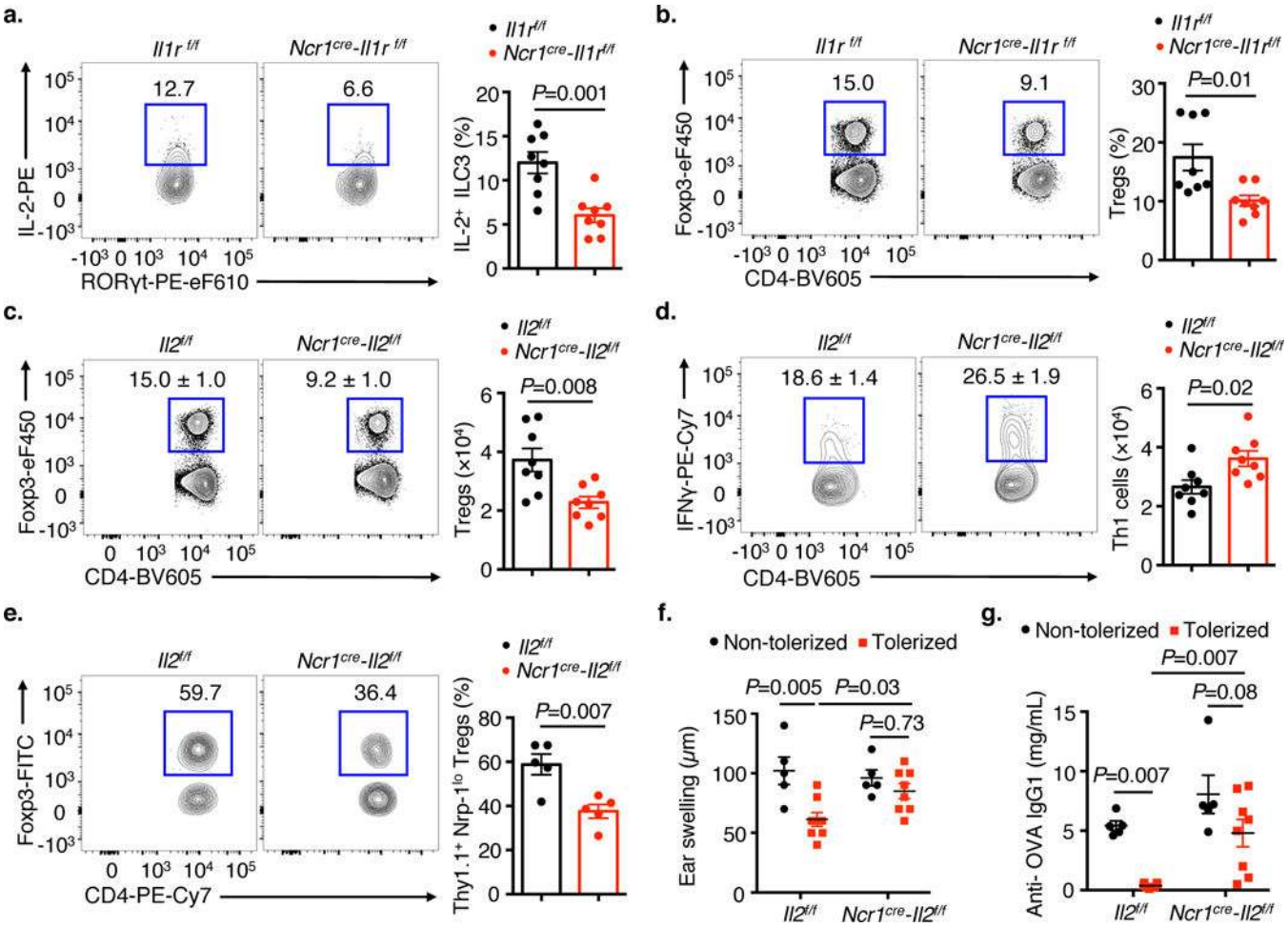

Figure 3. ILC3-derived IL-2 is essential for Tregs maintenance, immunological homeostasis and oral tolerance to dietary antigen in the small intestine.

a, **b**. Flow cytometry plots with graph of the frequencies of IL-2$^+$ ILC3 (**a**) or Tregs (**b**) in SI-LPs of *Il1r*$^{f/f}$ and *Ncr1*^{cre}-*Il1r*$^{f/f}$ mice (n=8). **c**, **d**. Flow cytometry plots and quantification of cell numbers of Tregs (**c**) and Th1 cells (**d**) in SI-LPs of *Il2*$^{f/f}$ and *Ncr1*^{cre}-*Il2*$^{f/f}$ mice at steady state (n=8). **e**. Naïve OT-II CD4$^+$ T cells were transferred into *Il2*$^{f/f}$ and *Ncr1*^{cre}-*Il2*$^{f/f}$ mice and recipient mice were fed with OVA for 12 days. Donor T cells were analyzed for Foxp3 staining in the SI-LPs (n=5). **f**, **g**. DTH response was assessed in designated mice by ear swelling (**f**) and serum concentration of anti-OVA IgG1 was tested by ELISA (**g**) (n=5 of non-tolerized group and n=8 of tolerized group). Data in **a-d**, **f** and **g** are pooled from two independent experiments. Data in **e** is representative of two independent experiments with similar results (at least 4 mice per group). Results are shown as the means ± s.e.m. Statistics are calculated by unpaired two-tailed Student's *t*-test (**a-e**) or two-way ANOVA (**f**, **g**). *P* values are indicated on the figure.

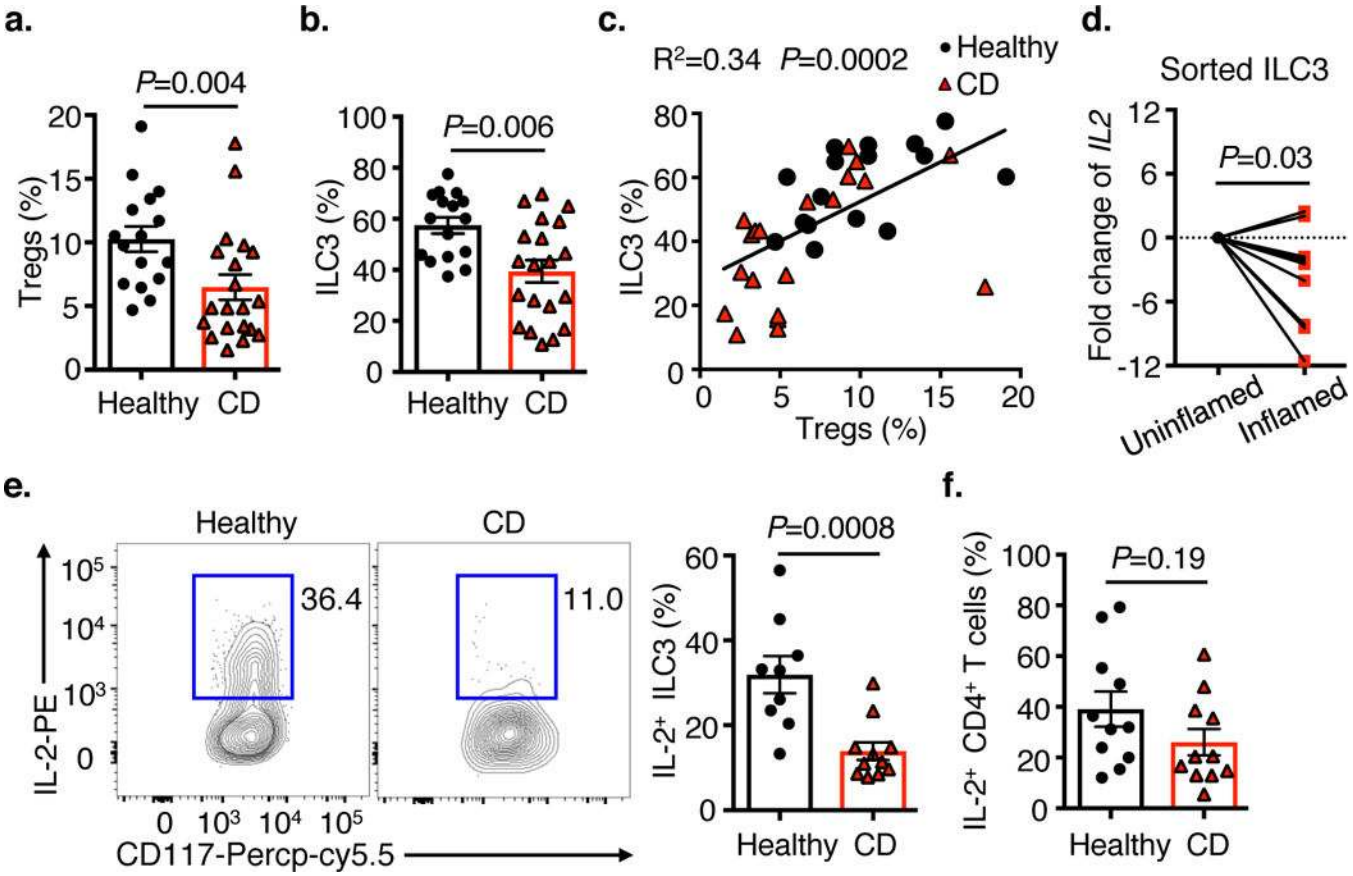

Figure 4. ILC3 production of IL-2 is impaired in the intestine of Crohn's disease patients.

a-f. Lamina propria cells were isolated from terminal ileum biopsies from healthy or Crohn's disease (CD) patients, and the frequency of Tregs ($CD45^+CD3^+CD4^+Foxp3^+$ of $CD4^+$ T cells) (**a**) and ILC3 ($CD45^+Lin^-CD127^+CD117^+NKp44^+$ of total ILCs) (**b**) were quantified. The frequency of ILC3 was correlated with the frequency of Tregs in (**c**) (n=16 healthy and n=20 CD patients). **d**. Human ILC3 were sort-purified from resected tissues of CD patients and *IL2* transcript was examined by qPCR. **e**, **f**. The frequency of IL-2^+ ILC3 (**e**) or IL-2^+ $CD4^+$ T cells (**f**) were analyzed in healthy controls (n=11) and CD patients (n=11) by flow cytometry. Data in **a-c**, **e** and **f**, statistical analyses performed using a Mann-Whitney test (unpaired). Correlative analyses were compared by parametric Pearson's rank correlation coefficient (r). Data in **d** is performed using Wilcoxon matched-pairs test (paired). Results are shown as the means ± s.e.m. Statistics are calculated by two-tailed test. *P* values are indicated on the figure.